Modeling boreal forest evapotranspiration and water balance at stand and catchment scales: a spatial approach

Samuli Launiainen[1], Mingfu Guan[2,1], Aura Salmivaara[1], and Antti-Jussi Kieloaho[1]

[1]Nature Resources Institute Finland, Latokartanonkaari 9, 00790 Helsinki, Finland
[2]Department of Civil Engineering, The University of Hong Kong, HKSAR, China

Correspondence: Samuli Launiainen (samuli.launiainen@luke.fi)

Abstract.

Vegetation is known to have strong influence on evapotranspiration (ET), a major component of terrestrial water balance. Yet hydrological models often describe ET by methods unable to include the variability of vegetation characteristics in their predictions. To take advantage of increasing availability of high-resolution open GIS-data on land use, vegetation and soil characteristics in the boreal zone, a modular, spatially distributed model for predicting ET and other hydrological processes from a grid cell to catchment level is presented and validated. An improved approach to upscale stomatal conductance to canopy scale using information on plant type (conifer / deciduous) and stand leaf-area index (LAI) is proposed by coupling a common leaf-scale stomatal conductance model with a simple canopy radiation transfer scheme. Further, a generic parametrization for vegetation-related hydrological processes for Nordic boreal forests is derived based on literature and data from a boreal FluxNet site. With the generic parametrization, the model was shown to well reproduce daily ET measured by eddy-covariance technique at ten conifer-dominated Nordic forests whose LAI ranged from 0.2 to 6.8 m^2m^{-2}. Topography, soil and vegetation properties at 21 small boreal headwater catchments in Finland were derived from open GIS-data at 16 x 16 m grid size to upscale water balance from stand to catchment level. The predictions of annual ET and specific discharge were successful in all catchments, located from 60 to 68 °N, and daily discharge also reasonably well predicted by calibrating only one parameter against discharge measurements. The role of vegetation heterogeneity on soil moisture and partitioning of ET was demonstrated. The proposed framework can support e.g. forest trafficability forecasting and predicting impacts of climate change and forest management on stand and catchment water balance. With appropriate parametrization it can be generalized outside the boreal coniferous forests.

1 Introduction

The boreal region, encompassing ca. 12 % of world's land area, is characterized by mosaic of peatlands, lakes and forests of different ages and structures. Landscape heterogeneity has major influence on hydrological cycle, carbon balance and land-

atmosphere interactions in the region (McDonnell et al., 2007; Govind et al., 2011; Stoy et al., 2013; Chapin et al., 2000; McGuire et al., 2002; Karlsen et al., 2016). Understanding spatial and temporal patterns of hydrological fluxes and state variables is becoming increasingly important in the context of intensifying use of boreal forests under the pressures from climate change (Bonan, 2008; Gauthier et al., 2015; Price et al., 2013; Spittlehouse, 2005; Laudon et al., 2016). Thus, model approaches that can effectively utilize available environmental data, open high-resolution GIS-data and remote-sensing products for hydrological predictions are necessary for climate-smart and environmentally sustainable use of boreal ecosystems (Mendoza et al., 2002).

Diverse modeling approaches are used to predict point scale, catchment and regional hydrological balance, which reflects the broad spectrum of practical needs and research questions addressed, as well as historical development of hydrological models. The approaches range from lumped rainfall-runoff schemes (Beven and Kirkby, 1979; Bergström, 1992) to semi- and fully-distributed physically-based models (Vivoni et al., 2011; Panday and Huyakorn, 2004; Ivanov et al., 2004; Ma et al., 2016; Clark et al., 2015a, b; Best et al., 2011; Niu et al., 2011; Ala-aho et al., 2017). Lumped models are often based on conceptual representation of hydrological processes and calibrated against a few integrative measures, such as stream discharge. They are computationally inexpensive but cannot well address spatial variability of hydrological fluxes and state variables within a catchment. Distributed mechanistic models, on the other hand, use first principles to predict water flow and state variables through the landscape and can incorporate topography, soil texture and vegetation heterogeneity in their predictions (Samaniego et al., 2010). However, high computational costs and challenges in estimating spatially variable parameters hampers their use and performance (Freeze and Harlan, 1969; Montanari and Koutsoyiannis, 2012; Grayson et al., 1992; Reed et al., 2004). It has been questioned whether fully distributed models are suitable for operative hydrological forecasts over large areas (Khakbaz et al., 2012) and semi-distributed models that combine physical and conceptual elements are often suggested as practical solutions (Khakbaz et al., 2012; Gao et al., 2013; Savenije, 2010).

The common scientific questions in hydrological modelling are, as proposed by Clark et al. (2015a), related to describing and parametrising water and energy fluxes and representing landscape variability and hydrological connectivity at the spatial and temporal scales of the model discretization. Availability of good-quality high-resolution open data on land use, topography, vegetation, and soil characteristics has increased significantly during the recent decade. In Finland for instance, high-accuracy digital elevation models (DEM's) are openly available at 2m and 10m resolution (NSLF, 2017), reasonably good soil maps cover the country at scale of 1:20 000 or 1:200 000 (GSF, 2015), and the multi-source National Forest Inventory (mNFI, Mäkisara et al. (2016); Kangas et al. (2018)) provides information on various forest and site type attributes at 16m resolution throughout the country. To take full advantage of open GIS data and fine-resolution (i.e. tens to hundreds of meters) remote-sensing products of hydrological fluxes and state variables (Ryu et al., 2011; Herman et al., 2018), computationally efficient models capable of accounting for landscape variability are necessary. Further, these models should be sufficiently generic in their parametrization and use standard meteorological data to allow their use on large, often data-sparse areas. As the appropriate level of detail is strongly driven by the research question or practical application at hand (Clark et al., 2011; Savenije, 2010), effective development of hydrological models requires moving from a specific model towards modular frameworks (Clark et al., 2015a; Wagener et al., 2001; Clark et al., 2011).

Increasing availability of high-resolution data on vegetation and its functioning paves way to improve description sof spatial and temporal variability of evapotranspiration (ET), a major component of terrestrial water balance. Within a specific biome and climatic region, vegetation characteristics such as species composition and leaf-area index (LAI) have major influence on variability of ET (Williams et al., 2012; Zeng et al., 2018; Launiainen et al., 2016). In modern land surface models, ET components are computed either using a big-leaf framework or by describing the microclimatic gradients and exchange rates explicitly throughout a multi-layer canopy-soil system and upscaling these directly to ecosystem scale (Katul et al., 2012; Bonan et al., 2014). In both cases upscaling of stomatal conductance g_s and transpiration rate from leaf to canopy scale is based on physical arguments, and constrained by plant carbon economy (Cowan and Farquhar, 1977; Katul et al., 2012; Medlyn et al., 2012) and hydraulic architecture (Sperry, 2000; Tyree and Zimmermann, 2002). The non-linear dependency of ET components on vegetation characteristics and microclimate, however, remain mostly unresolved or are highly parametrised in most hydrological models, where the bulk ET is commonly computed by using Penman-Monteith equation or as a crop or vegetation type dependent fraction of potential evaporation (Zhao et al., 2013; Fisher et al., 2005; Allen et al., 1998). Thus, improving ET description by more physiologically-phased approach can be proposed as one potential area to reduce uncertainties in predictions of hydrological budget and resulting streamflow and soil moisture patterns.

Motivated both by scientific needs and potential practical applications, this study addresses two independent but inter-related objectives: First, we develop a generic model for daily ET in boreal forest and peatland ecosystems, and explore how daily and annual ET can be predicted based on plant functional traits, canopy LAI and open data on landscape structure and meteorological forcing. We distinguish between evaporative fluxes and transpiration, and predict canopy conductance G_c and canopy transpiration rate by coupling the unified stomatal model (Medlyn et al., 2012) with simplified canopy radiative transfer theory (Saugier and Katerji, 1991; Kelliher et al., 1995; Leuning et al., 2008). We perform parameter sensitivity analysis and validate the model predictions against eddy-covariance (EC) measurements of stand-scale ET at ten boreal forest and peatland sites in Finland and Sweden (Launiainen et al., 2016).

Second, we extend the analysis to catchment scale and propose modular, semi-distributed Spatial Forest Hydrology (SpaFHy) model for predicting spatial and temporal patterns of hydrologic fluxes and state variables across the boreal catchments. The SpaFHy aims to provide reasonably simple, practically applicable and extensible framework that can effectively use open GIS data and basic meteorological data. We apply SpaFHy to 21 headwater catchments located throughout Finland to validate its predictions against daily stream discharge and annual ET derived from catchment water balance. Spatial variability of ET, snow water equivalent (SWE) and soil moisture, and temporal variability of stream discharge are demonstrated and potential applications finally discussed. Although developed for boreal ecosystems, the proposed methods can be extended to other biomes with appropriate parametrizations.

2 Model description

SpaFHy framework consists of three sub-models (Fig. 1). Hydrological processes in vegetation and two-layer topsoil are explicitly modelled for each grid cell, while Topmodel concept (Beven and Kirkby, 1979) is used to link grid cell and catchment

water budgets, and to describe baseflow and returnflow generation mechanisms. The SpaFHy submodels and equations are presented in the next sections, and complemented in Supplementary material. Throughout, we use notation where angle parenthesis $\langle y \rangle$ indicate spatial and $\overline{y}$ temporal averages of quantity y, and units mm correspond to kg H_2O m^{-2} of surface area.

2.1 Canopy sub-model: above-ground water budget and fluxes at a grid cell

Hydrological processes in vegetation canopy, forest floor, snowpack, and in organic moss/humus layer and underlying root zone are solved for each grid cell using information on stand structure and soil type (Fig. 1; *Canopy* and *Bucket* -submodels).

2.1.1 P-M equation and ET

Total evapotranspiration is defined as sum of physiologically controlled transpiration (T_r) and physically regulated evaporation from wet canopy (E) and forest floor (E_f). To account for different controls of these processes, a three-source model is applied to describe ET at a grid-cell scale (Fig. 1). The Penman-Monteith (hereafter referred as P-M) equation gives each component of ET (mm d^{-1}) as (Monteith and Unsworth, 2008)

$$E_i = \frac{1}{\rho_w L_v} \frac{\Delta A_e + \rho_a c_p G_a D}{\Delta + \gamma(1 + G_a/G_i)} \Delta t, \tag{1}$$

where L_v is latent heat of vaporization (J kg^{-1}), Δ and γ (Pa K^{-1}) slope of saturation vapor pressure curve and psychrometric constant, respectively, ρ_w and ρ_a are densities of liquid water and air (kg m^{-3}), c_p is the heat capacity of dry air at constant pressure (J kg^{-1} K^{-1}), D is the vapor pressure deficit at air temperature (Pa) and A_e is the available energy (W m^{-2}), and Δt daily timestep (86400 s). Depending on specific ET component E_i, the surface conductance G_i (m s^{-1}) and aerodynamic conductance G_a have different forms. For canopy layer, which contributes to T_r and E, the G_a represents efficiency of within-canopy turbulent transport and transport through laminar boundary layers on leaf surfaces, and is computed as a function of wind speed U, canopy height h_c and LAI (Magnani et al., 1998; Leuning et al., 2008) (Suppl. S2).

2.1.2 Transpiration and canopy conductance

To calculate T_r and resulting water uptake from the root zone, an estimate of the canopy conductance G_c is needed. Analysing large corpus of leaf gas-exchange data through stomatal optimization arguments, Medlyn et al. (2012) proposed that leaf-scale stomatal conductance (g_s, mol m^{-2} s^{-1}) is related to leaf net photosynthetic rate (A, μmol $m^{-2}s^{-1}$) as

$$g_s = g_o + 1.6 \left(1 + \frac{g_1}{\sqrt{D}}\right) \frac{A}{C_a}, \tag{2}$$

where C_a is the atmospheric CO_2 mixing ratio (ppm), D (kPa) is vapor pressure deficit, g_o residual (or cuticular) conductance and g_1 a species-specific parameter that depends on plant water use strategy. Noting that $g_o \ll g_s$ (Medlyn et al., 2012) and representing photosynthetic light response by saturating hyperbola (Saugier and Katerji, 1991), eq. (2) can be approximated as

$$g_s = 1.6 \left(1 + \frac{g_1}{\sqrt{D}}\right) \frac{A_{max}}{C_a} \frac{PAR}{PAR + b} C_{air}, \tag{3}$$

where A_{max} (μ mol m^{-2} s^{-1}) is the light-saturated photosynthesis rate, b (W m^{-2}) the half-saturation value of photosynthetically active radiation (PAR), and molar density of air C_{air} (mol m^{-3}) converts units of g_s to m s^{-1}.

Assuming PAR decays exponentially within the canopy, $PAR(L) = PAR_o \exp(-k_p L)$ (where L is the cumulative leaf area from canopy top, k_p the attenuation coefficient and PAR_o the incoming PAR above canopy) and neglecting vertical variations in D, eq. (3) can be integrated analytically over L yielding canopy conductance (m s^{-1}) as

$$G_c = \left[1.6\,(1 + \frac{g_1}{\sqrt{D}})\frac{A_{max}}{C_{a,ref}}\right] \left(\frac{1}{k_p}\frac{PAR_o + b}{PAR_o \times \exp(-k_p LAI) + b/k_p}\right) C_{air} \times f(\theta_{rew}) \times f_Y, \tag{4}$$

where the first term of eq. 4 is the canopy-scale light and D response, the $f(\theta_{rew})$, and f_Y (-) are dimensionless scaling factors introduced to represent the effect of soil moisture availability (eq. 6) and phenology (eq. 8). Equation (4) shows that at a given LAI, G_c is constrained leaf by leaf water use traits (via g_1), and photosynthetic capacity and light-response (via A_{max} and b). Such traits are readily measurable by leaf gas-exchange and widely available in literature and in plant trait databases such as TRY (Kattge et al., 2011). Derivation of parameters is presented and predictions of eq. 4 compared against a common gas-exchange model in Suppl. S3.

Water use strategies and to lesser extent photosynthetic capacity of common coniferous and deciduous species in boreal forests differ (see e.g. Lin et al. (2015)). Thus, LAI-weighted effective values of g_1 and A_{max} are calculated for a grid cell as

$$p = (1 - f_d)\,p_c + f_d\,p_d \tag{5}$$

where p is the parameter, the subscript c and d refer to conifer and deciduous trees, respectively, and $f_d = LAI_d/(LAI_c + LAI_d)$ the contribution of deciduous trees on total LAI. Seasonal cycle of LAI_d is described using scheme based on accumulated degree-days (Launiainen et al., 2015) calibrated using leaf phenology observations in Southern and Northern Finland.

The effect of soil moisture availability on G_c is based on sap-flow study on Scots pine and Norway Spruce in central Sweden (Lagergren and Lindroth, 2002)

$$f(\theta_{rew}) = \begin{cases} \frac{\theta_{rew}}{x_r}, & \theta_{rew} < x_r \\ 1, & \theta_{rew} \geq x_r, \end{cases} \tag{6}$$

where θ_{rew} (m^{3}m^{-3}) is relative plant available water θ_{rew}, and x_r (m^{3}m^{-3}) threshold below which reduction in G_c occurs. θ_{rew} relates volumetric water content θ (-) in the root zone to soil-type depended field capacity (θ_{fc}) and wilting point (θ_{wp}) as

$$\theta_{rew} = \frac{\theta - \theta_{wp}}{\theta_{fc} - \theta_{wp}}. \tag{7}$$

The phenology factor f_Y (-) describes seasonal acclimation of photosynthetic capacity as a function of delayed temperature sum (Kolari et al., 2007a)

$$f_Y(t) = \max\left[0.1, \min\left(1, \frac{Y(t) - T_{0,y}}{Y_{max} - T_{0,y}}\right)\right], \tag{8}$$

where t is time, $Y(t)$ ($^\circ C$) describes the stage of development (Kolari et al., 2007b), $T_{0,y}$ a threshold temperature and Y_{max} the value at which full recovery of photosynthetic capacity occurs. The Y is accumulated from the beginning of the year and its rate of change is

$$\frac{dY}{dt} = \frac{\overline{T_a} - T_{0,y}}{\tau}, \tag{9}$$

where τ is time constant of the recovery (Table 1).

2.1.3 Evaporation from forest floor

Forest floor evaporation E_f is extracted from the organic moss/humus layer on top of root zone (Fig. 1). We compute E_f (mm d^{-1}) as

$$E_f = f \times E_{f,0}, \tag{10}$$

where $E_{f,0}$ is evaporation rate when moisture supply in the organic layer does not limit E_f, and is calculated by eq. 1 where $R_n = R_{n,o} \exp^{-k_p\, LAI}$ ($R_{n,o}$ is net radiation above canopy), G_a depends on surface roughness length and modeled U 0.5 m above the forest floor and G_i now represents the conductance of saturated ground surface (G_f) and is calibrated against EC data from a boreal fen as described later. The factor f accounts for the decay of E_f in drying organic matter as

$$f = \begin{cases} \frac{\theta_{org}}{x_{r,o}}, & \theta_{org} < x_{r,o} \\ 1, & \theta_{org} \geq x_{r,o}, \end{cases} \tag{11}$$

where θ_{org} ($\mathrm{m}^2\mathrm{m}^{-2}$) is organic layer water content, and $x_{r,o} = 0.8\theta_{fc,org}$ based on linear decrease of moss evaporation below threshold moisture content (Williams and Flanagan, 1996).

2.1.4 Interception, throughfall and evaporation from canopy storage

Canopy water storage is described as a single pool filled by interception I_c of precipitation and snowfall (P), and drained by evaporation/sublimation E and snow unloading U_s (all in mm d^{-1}). The change in canopy water storage W (mm) is

$$\frac{\Delta W}{\Delta t} = I_c - E - U_s. \tag{12}$$

The interception sub-model assumes that full storage is approached asymptotically (Aston, 1979; Hedstrom and Pomeroy, 1998)

$$I_c = (W_{max} - W_0)\left(1 - e^{-\frac{c_f}{W_{max}} P\, \Delta t}\right), \tag{13}$$

where c_f (-) is the canopy closure, W_0 the initial water storage, and the canopy storage capacity $W_{max} = w_{max}\, LAI$ (mm) linearly proportional to LAI. The empirical storage parameter w_{max} (mm LAI^{-1}) is known to be greater for rain and snow (Koivusalo and Kokkonen, 2002); if W exceeds W_{max} of liquid water and daily mean temperature is above zero, the excess

snow storage is removed as snow unloading and added into throughfall input to snow model. In snowfree conditions, all throughfall is routed to forest floor surface and provides input to *Bucket* sub-model.

Evaporation / sublimation from canopy storage is calculated by P-M equation (eq. 1), where the G_a is defined as for T_r while the canopy surface conductance G_i set infinite for evaporation from wet canopy, and computed for snow sublimation as in Essery et al. (2003) and Pomeroy et al. (1998) (Suppl. S4).

2.1.5 Snow accumulation and melt

Snowpack on the ground is modelled in terms of snow water equivalent (SWE, mm), a lumped storage receiving throughfall and unloading from the canopy and releasing water by snowmelt. The melt rate M (mm d^{-1}) is based on temperature-index approach

$$M = \min[SWE,\, K_m\,(T_a - T_o)], \tag{14}$$

where $T_o = 0.0°C$ is threshold temperature and T_a daily mean air temperature. The melting coefficient K_m (mm d^{-1} $°C^{-1}$) decreases with increasing canopy closure as Kuusisto (1984)

$$K_m = K_{m,o} - 1.64\,c_f, \tag{15}$$

where $K_{m,o}$ is the melting coefficient at open area. The snowpack can retain only a certain fraction of liquid water (Table 1 and Suppl. S4), and excess is routed to soil module.

2.2 Bucket model: topsoil water balance

The topsoil water balance at each grid cell is described as a two-layer bucket model (*Bucket*, Fig. 1). An organic layer of depth z_{org} (mm), representing living mosses and poorly decomposed humus, overlies the root zone and acts as an interception storage for throughfall and snowmelt. Its volumetric water content θ_{org} (m^{3}m^{-3}) is bounded between field capacity $\theta_{fc,org}$ and residual water content $\theta_{r,org}$ and vary according to

$$\frac{\Delta\theta_{org}}{\Delta t} = \frac{I_{org} - E_f + Q_{r,ex}}{z_{org}}, \tag{16}$$

where I_{org} is interception rate, restricted either by throughfall or available storage space, and $Q_{r,ex}$ returnflow from the hillslope through the rootzone described below. All E_f is extracted from the organic layer.

The water content θ in the root zone of depth z_z (mm) changes according to

$$\frac{\Delta\theta}{\Delta t} = \frac{I_f - T_r - D_r + Q_r}{z_s}, \tag{17}$$

where infiltration I_f (mm d^{-1}) and returnflow from the catchment sub-surface storage (sect. 2.3) Q_r provide input, and T_r, and drainage D_r outflows from the root zone. The maximum water storage is determined by root zone depth z_s and porosity θ_s, and I_f restricted either by potential infiltration or available storage space. In case of infiltration or returnflow excess, the organic layer storage is first updated, and remaining routed to stream outlet without delay as surface runoff (Q_s).

Drainage D_r (mm d^{-1}) from root zone occurs whenever θ is above field capacity θ_{fc} as (Campbell, 1985)

$$D_r(\theta) = \begin{cases} K_{sat} \left(\frac{\theta}{\theta_s}\right)^{2\beta+3}, \theta > \theta_{fc}, \\ 0, \theta \leq \theta_{fc}, \end{cases} \tag{18}$$

where the saturated hydraulic conductivity K_{sat} (mm d^{-1}) and its decay parameter β depend on soil type.

2.3 Topmodel: integration from point to catchment level

To achieve computational efficiency and applicability at large-scale, lateral flow in the saturated zone is not explicitly solved but grid-cell and catchment water balances conceptually linked by Topmodel approach (Beven and Kirkby, 1979). In *Topmodel*, the catchment sub-surface storage is described as a single bucket (Fig. 1). The change in the average saturation deficit $\langle S \rangle$ (mm), i.e. the average amount of water per unit area required to bring the catchment sub-surface storage (below the root zone) to saturation, is

$$\frac{\Delta \langle S \rangle}{\Delta t} = -\langle D_r \rangle + \langle Q_b \rangle + \langle Q_r \rangle, \tag{19}$$

where $\langle D_r \rangle$ (mm d^{-1}) is catchment average root zone drainage, $\langle Q_b \rangle$ (mm d^{-1}) the catchment baseflow and $\langle Q_r \rangle$ (mm d^{-1}) average return flow from the sub-surface storage. Assuming soil transmissivity is spatially uniform and decays exponentially with depth, the $\langle Q_b \rangle$ becomes (Beven, 1997)

$$\langle Q_b \rangle = Q_o \exp^{-\langle S \rangle / m} = T_o \exp^{-\langle TWI \rangle} exp^{-\langle S \rangle / m}, \tag{20}$$

where m (mm) is a scaling parameter reflecting the effective water-conducting soil depth, T_o the soil transmissivity at saturation, and Q_o (mm d^{-1}) baseflow rate when $\langle S \rangle$ is zero. The $\langle TWI \rangle$ represents the catchment average of local topographic wetness index TWI defined by the natural logarithm of the area draining through a grid cell a from upslope and tangent of the local surface slope α (Beven and Kirkby, 1979)

$$TWI = \ln\left(\frac{a}{\tan\alpha}\right). \tag{21}$$

The saturation deficit S (mm) of a grid cell is uniquely related to $\langle S \rangle$ by

$$S = \langle S \rangle + m\left(\langle TWI \rangle - TWI\right), \tag{22}$$

which implies that grid cells with high TWI have higher probability to become saturated, and the catchment saturated area fraction is related both to TWI distribution and to amount of water in the catchment sub-surface storage. Furthermore, eq. 21 shows high value of TWI can result either from large contributing area or flat local topography.

At grid cells where saturation excess ($S < 0$) occurs, returnflow $Q_r = -S/\Delta t$ from the sub-surface storage is routed through the rootzone and organic layer and their water storages are sequentially updated at next Δt. This creates an approximate feedback from local S, controlled by catchment water storage and topography, to topsoil water budget (sect. 2.2) and delays drying of root zone and organic layer at lowland grid cells receiving Q_r from the hillslope.

Specific discharge Q_f (mm d^{-1}) at catchment outlet is finally computed as

$$\langle Q_f \rangle = \langle Q_b \rangle + \langle Q_s \rangle \,, \tag{23}$$

where $\langle Q_s \rangle$ is the catchment average surface runoff (sect. 2.2).

2.4 Model inputs

SpaFHy requires daily mean air temperature T_a (°C), global radiation R_g (Wm^{-2}), relative humidity RH (%), wind speed (m s^{-1}) and daily accumulated precipitation P (mm d^{-1}) as forcing. The forcing can be either spatially uniform or vary for each grid cell in the spatial simulations. Available energy is computed from R_g accounting for the effect of LAI on R_n (Fig. 2a in Launiainen et al. (2016)), and PAR$_o = 0.5 \times R_g$.

The model requires following variables to be provided at user-defined grid:

1. Canopy and Bucket -submodels
   - Conifer and deciduous tree 1-sided leaf-area index (LAI$_c$ and LAI$_d$, respectively)
   - canopy height h_c (m)
   - Organic layer depth, root zone depth and hydraulic properties (Table S1)
2. Topmodel -submodel
   - topographic wetness index TWI
   - masks of catchment area and permanent water bodies

All the above variables are derived from open GIS-data available throughout Finland. The SpaFHy structure is modular and the three sub-models are linked via water fluxes, and feedbacks based on state variables such as θ_{rew} (Fig. 1). Each sub-model can thus be used stand-alone when appropriate forcing data is provided. The model is written in pure Python 2.7/3.6 and uses element-wise operations of Numpy -arrays for all computations. The GIS-data for model initialization are given as raster arrays, while NetCDF -format is used for storing the model outputs that include daily grids of all state variables and fluxes.

2.5 Model parametrization and sensitivity analysis at stand scale

Parameters required by each sub-model are given in Table 1 with their generic values. We applied a sequential approach to determine the generic parameter set to describe above-ground hydrology of coniferous-dominated landscape. First, we derived likely ranges of *Canopy* sub-model parameters from the literature and predictions of a common leaf gas-exchange model (Suppl. S3). The rainfall interception capacity was calibrated against spatially averaged throughfall measurements (2001 - 2010) made at the Hyytiälä research station in Juupajoki, Southern Finland (FIHy; Table. 2, Fig. 2). An overview of the site is given by Hari and Kulmala (2005) while Ilvesniemi et al. (2010) describe the hydrological measurements. The parameter f in surface conductance for evaporation from wet soil surface (G_f, eq. 10) was calibrated against eddy-covariance based ET

from a boreal fen site (FISii, Alekseychik et al. (2017)) located next to FIHy (Table 2). Monte-Carlo simulations (n=100), where parameter candidates were sampled from uniform distribution and objective function was set to minimize bias between modelled and measured values, were performed.

After parameter ranges were determined, global sensitivity analysis was performed to identify the key parameters controlling annual ET and its components, and annual maximun SWE. For this analysis, the *Canopy* and *Bucket* modules were coupled and the resulting stand-scale model run with various parameter combinations using daily forcing data from FIHy site (2000-2010) as input. We used Morris method, a global extension of elementary effect test used to determine which model parameters are negligible, linear and additive, or non-linear or involved in interactions with other parameters (Morris, 1991; Campolongo et al., 2007). In the Morris method, three sensitivity measures are calculated from distribution of scaled elementary effects. The mean of distribution (μ) is the overall effect of a parameter on the output, and the standard deviation (σ) is effect of a parameter due to non-linearity or due to interactions with other parameters. Third measure is the mean of the distribution of the absolute values of the elementary effects ($\mu^\star$) that provides ranking of parameters which is not biased by possible non-monotonic behavior of the model. The sensitivity measures are interpreted graphically together with rank parameters according to their overall influence; the intuitive interpretation is that the greater the absolute value of the measure the more important the parameter is for the studied model output. To ease graphical interpretation, standard error of the mean as $SEM = \sigma/\sqrt{r}$, where r is the number of trajectories, was estimated and used as suggested by Morris (1991). Analysis was conducted by using a Python package SALib (v. 1.1.2; Herman and Usher, 2017).

The ranges of the 14 parameters considered in the sensitivity analysis are listed in Table 3. In the analysis, leaf area indices for conifers and deciduous were calculated from total 1-sided LAI and deciduous fraction. Each parameter was allowed to vary over eight levels, and 60 optimal trajectories were generated from 600 initial trajectories by the sampling scheme introduced by Ruano et al. (2012). In total, 900 samples were generated and the number of optimal trajectories was determined following Ruano et al. (2011).

After sensitivity analysis, most of the parameters could be fixed (those deemed less-influential), and only the 'generic' values for A_{max} and g_1 in eq. (4) were confirmed by calibrating them against eddy-covariance (EC) -measured ET (years 2005 - 2007) at FIHy -site. The possible ranges of these parameters were constrained by physiological arguments. Monte-Carlo simulations (N=100), where parameters were sampled from uniform distribution and objective function was set to minimize bias between modelled and measured daily ET were performed. We considered only dry-canopy conditions, i.e. no rain during the current or previous day.

2.6 Model validation at stand scale

To validate how daily ET can be predicted across LAI, sitetype and latitudinal gradient using a single parameter set (Table 1), the stand-level model was run using daily meteorological data from nine additional EC-flux sites in Finland and Sweden (Table 2, Fig. 2). The sites range from dense mixed coniferous forests (SENor) to recently harvested stand (FICage4) and pristine fen peatland site (FISii), and the measurements, flux calculation and data post-processing have been described elsewhere (Launiainen et al., 2016; Minunno et al., 2016). For each site, LAI_c, LAI_d, h_c and soil properties were set according to

measured/inferred values, and predicted daily growing-season (May-Oct) ET in dry-canopy conditions ($ET \simeq T_r + E_f$) was compared to measured. At FIHy, the soil moisture in the root zone was measured continuously, and SWE recorded bi-weekly during five winters and used to compare respective model predictions.

2.7 Model validation at catchment scale

To address how well SpaFHy can predict daily specific discharge and annual partitioning of P into ET and Q_f at catchment scale, we applied the model to 21 small boreal headwater catchments located throughout Finland (Fig. 2, Table S2) using same generic parameter set as in the stand-level validation (Table 1). All the catchments belong to the Finnish network for monitoring water quality impacts of forestry (Finér et al., 2017), and their characteristics can be found in Supplementary material (Table S2). Water levels at v-notch weirs were measured continuously at the catchment outlets by limnigraphs or pressure-sensors, and manual reference measurements were taken ca. 20 times per year adjacent to water quality sampling and used to calibrate the weir water level data whenever necessary. Weir equations and catchment area were used to convert water level to specific discharge Q_f. In absence of *in-situ* weather data, daily 10 x 10 km grid data provided by Finnish Meteorological Institute were used as model forcing taking values from a gridpoint nearest to the catchment outlets. Since wind speed was not available, it was set to constant value of 2 ms^{-1} resembling annual mean 2 m wind speed in Finland.

2.7.1 Processing of GIS -data

Example of GIS-data used to set up the model for catchment C3 Porkkavaara in Eastern Finland are shown in Fig. 3. The catchment boundaries and TWI were derived from DEM provided by National Survey of Finland (NSLF, 2017). The DEM original resolution was 2 m or 10 m depending on catchment location. The resolution was aggregated with the mean elevation value into 16 m resolution which corresponds to the resolution of the multi-source National Forest Inventory of Finland (mNFI) data. The mNFI data provides essential data layers for the model, e.g. stand volume, basal area, mean height, age, site fertility class and estimates of root, stem, branch and needle/leaf biomasses for pine, spruce and aggregated deciduous trees at 16 m resolution throughout Finland Mäkisara et al. (2016).

The DEM pre-processing, defining of the catchment boundaries and calculation of TWI based on the aggregated DEM were conducted in WhiteBox GIS programme (Lindsay, 2014). Pre-processing included consideration of the road and stream intersections derived from the Topographical Database (NSLF, 2017), which were burned into the DEM to account for culverts and ensure continuous stream network. Further, all water elements were burned into the DEM with 1 meter upper threshold and a decay factor accounting for possible miss-aligned stream data. Filling of artificial pits in DEM was conducted using 'Fast Breach Depressions' tool (Lindsay, 2016) and the flow direction and flow accumulation (a) rasters were calculated with the D-infinity method (Tarboton, 1997). The TWI was finally calculated by eq. 21 and small lakes within the catchments, derived from the Topographic Database (NSLF, 2017), were reset as nodata and omitted from further computations. The needle and leaf mass rasters were converted into LAI_c and maximum deciduous tree LAI $LAI_{d,max}$ using specific 1-sided leaf-areas for pine, spruce and birch (6.8, 4.7 and 12.0 m^2 kg^{-1}, respectively; Härkönen et al. (2015)). The canopy closure and h_c were obtained directly from the mNFI data.

Topsoil classification was derived from soil maps and peatland boundaries. Soil information is provided for parts of Finland in 1:20 000 scale while the whole Finland is covered with a coarser 1:200 000 scale soil map (GSF, 2015). Peatland classification is available as detailed polygon elements from the Topographical Database. The soil information were transformed to the 16 m grid based on the majority principle, and then re-classified into four classes: coarse, medium and fine-textured mineral and organic peat soils whose hydrologic properties are given in Table S1. Fine-textured soils correspond to clayey and silt soils, whereas coarse-textured are fine sand and coarser. Majority of the mineral soils in the study catchments belong to the medium-textured class (Table S2).

2.7.2 Calibration of Topmodel against specific discharge

Catchment-specific calibration was performed to determine the effective soil depth m of *Topmodel*, a parameter that defines the shape of Q_f recession and catchment average storage deficit $\langle S \rangle$ (eq. 22). The parameter T_o was fixed to 0.001 ms^{-1} since it was found not markedly affect the model performance, as also observed elsewhere (Beven, 1997). The m was calibrated against measured daily specific discharge using Monte-Carlo sampling from uniform distribution (N=100). We used modified Willmott's index of agreement (Krause et al., 2005) as an objective function to quantify the goodness of fit

$$d_j = 1 - \frac{\sum_{i=1}^{n} \left| \langle Q_{m,i} \rangle - \langle Q_{f,i} \rangle \right|}{\sum_{i=1}^{n} \left| \langle Q_{m,i} \rangle - \langle \overline{Q_m} \rangle \right|}, \tag{24}$$

where d is in a range of 0 to 1, the higher the value, the better the match is; $\langle Q_{f,i} \rangle$ and $\langle Q_{m,i} \rangle$ are modelled and measured specific discharges at day i, and $\overline{\langle Q_m \rangle}$ represents temporal average of the measurements. This model goodness statistics provided visually determined better fits of streamflow recession than other commonly used statistical criteria; e.g. Nash-Suchliffe model efficiency was overly sensitive to high-flow peaks and affected by potential biases in P. The initial state of the model was set through one year spin-up period. The value of m significantly affected the dynamics of specific discharge $\langle Q_f(t) \rangle$ and $\langle S(t) \rangle$ but had negligible impact on catchment $\langle \overline{ET} \rangle$ or $\langle \overline{Q_m} \rangle$ at annual scale.

3 Results

3.1 Sensitivity analysis at stand scale

The sensitivity measures μ and σ for maximum SWE and annual ET and its components are shown in Table 4, and the ranking of parameters (via $\mu_\star$) in Supplementary Fig. S1.

Total LAI was ranked the most influential parameter for all studied *Canopy* sub-model outputs. In addition to LAI, the parameters that affect leaf level water use (g_1, z_s, A_{max}, and b) were among the most influential parameters for total ET and transpiration. The most influential parameters for ground evaporation E_f were LAI and k_p, which jointly define radiation availability at the ground. LAI also affects wind speed and thus aerodynamic conductance at the ground layer. In addition, surface conductance for wet forest floor G_f and $z_{s,org}$ and $\theta_{fc,org}$ that define water storage capacity of the organic layer were significant for E_f. The most influential parameters for interception evaporation E were LAI, w_{max}, f_d, h_c, and $w_{max,snow}$

that define interception capacity and subsequent evaporation/sublimation of rain and snow. The most influential parameters affecting annual maximum snow water equivalent were LAI, $w_{max,snow}$, f_d, w_{max}, and h_c.

LAI had also the largest σ meaning either interactions with other parameters or strong non-linearity. In case of ET and T_r, the coefficient of variation (σ / $\mu^\star$ -ratio) was over 1.0 and for E, E_f, and SWE it was smaller but over 0.5. The most influential parameters of all studied outputs had the coefficient of variation over 0.5. Non-monotonic behavior (i.e. μ / $\mu_\star$ -ratio is significantly different from unity) of the model was only observed in case of ET for LAI.

3.2 Validation at stand-scale

Predicted daily dry-canopy ET and root zone moisture content are compared against 10 years of measurements at the pine-dominated FIHy -site in Fig. 4. The results indicate the model reproduces well the observed seasonal patterns of ET and θ both during calibration (2005 - 2007) and validation period. The regression plots indicate ET predictions have negligible bias and well represent the variability, while the soil moisture changes are not fully captured. The SWE was also well reproduced by snow model parametrized by literature values (Pomeroy et al., 1998; Essery et al., 2003).

ET predictions for the nine additional EC-sites are shown in Fig. 5. The growing season (doy 120 - 273) dry-canopy ET is reasonably well predicted compared to independent observations across broad LAI -range (from 0.7 to 6.8 $\mathrm{m^2 m^{-2}}$) and over latitudinal and site-type gradient (Table 2, Fig. 2). At the youngest, recently clearcut site FICage4 the model underestimates ET, while slight overestimation is observed in particular at the northernmost, old-growth Scots pine site on coarse textured soil (FISod). In terms of explained variability, the model performance is the weakest at SESky2 (spruce), FIKal and FILet (drained peatland forests), potentially because ill-represented moisture limitations of transpiration and/or that of E_f. The non-linear behavior at SENor and less clearly at SESky2 and FILet is primarily caused by slower than observed spring recovery at these sites having high abundance of Norway spruce. As the Norway spruce has observed to recover more rapidly from winter dormancy than pine (Linkosalo et al., 2014; Minunno et al., 2016), this can be partly related to biased phenology-model that is based on Scots pine (Kolari et al., 2007a).

Also ET at the pristine fen peatland site FISii, where $E_f \gg T_r$, was accurately predicted when moisture limitation of E_f was neglected ($f = 1$ in eq. 10). Such case can be expected due to strong capillary connection between peat moss (*Sphagnum sp.*) and shallow water table maintained by lateral inflows from the surrounding landscape and weak drainage (Rouse, 1998; Ferone and Devito, 2004). When the organic layer moisture content feedback to E_f was activated, ET at FISii was frequently underestimated during summer dry spells (not shown); in point-scale simulations this represent the case where the organic layer water storage is recharged only by P.

Overall, the model performance at stand scale was satisfactory and dry-canopy ET well predicted over range of forest sites and climatic gradient in Finland. This suggests that the proposed three-source ET formulation and its generic parametrization for T_r, E_f and snow interception should be scalable over landscape scale variability of LAI, site types and latitude-driven weather forcing. Since EC measurements are know to be problematic during rainfall events (van Dijk et al., 2015; Kang et al., 2018), the comparison of stand-level ET was restricted to dry-canopy conditions.

3.3 Catchment water balance and specific discharge

On annual scale, changes in catchment water storage are negligible compared to annual $\langle ET \rangle$ and $\langle Q_f \rangle$, and water balance approach provides an independent check for the upscaled ET predictions at catchment level. Fig. 6 shows the comparison of modelled and water-balance based annual evapotranspiration fraction $\left\langle \overline{ET}/\overline{P} \right\rangle$ for the 21 headwater catchments across Finland (Fig. 2, Table S2). Results show a close agreement between measured and modelled P partitioning across the catchment space, especially considering the uncertainties in both axis. The uncertainty range of modelled $\left\langle \overline{ET}/\overline{P} \right\rangle$ implies the impact of model parameter uncertainty. The uncertainty range in Fig. 6 was derived by varying the most influential parameters for total ET and its partitioning (LAI, g_1, w_{max}, $w_{max,snow}$) by $\pm$ 20 % and grouping the combinations into 'high' and 'low' ET scenarios, respectively. While the model is mass-conserving, uncertainty of $\left\langle \overline{ET}/\overline{P} \right\rangle$ derived from catchment water balance is linearly proportional to uncertainty of Q_f derived from streamflow measurements and catchment area. Also systematic and random errors in the annual P cause respective uncertainties in $\left\langle \overline{ET}/\overline{P} \right\rangle$. In Fig. 6 the horizontal errorbars correspond to modest 10 % uncertainty assumed for P and catchment area.

Overall, the model predictions are reasonably good across the catchment space. Stepwise linear regression was tested to explain the annual residuals by catchment characteristics in Table S2 but no significant relationships were found. Also inter-annual variability of $\left\langle \overline{ET}/\overline{P} \right\rangle$ was well captured for majority of the catchments (not shown).

Figure 7 shows specific discharge and modelled soil moisture at catchment C3 Porkkavaara in Eastern Finland (Table S2), over two years characterized by wet (2012, P 452 mm in June-Sept) and dry (2013, P 246 mm) growing seasons. In 2012, the high snow accumulation resulted into stronger streamflow peak, and frequent rainfall events kept the catchment average root zone moisture $\langle \theta \rangle \geq 0.3$ m^{2}m^{-2} throughout the year. Also Q_f remained significantly higher throughout the summer compared to 2013, and responded rapidly to rainfall. During the drier 2013, transpiration depleted the root zone moisture well below field capacity and $\langle \theta \rangle$ dropped frequently to $\sim$0.15 m^{2}m^{-2} in June - August. The model was well able to predict spring Q_f peaks and recession curve, and also rainfall-induced peaks during the wet summer. During drier conditions, however, the small-magnitude peaks in summer Q_f were not well captured by the model. This suggests too high *Bucket* storage capacity and thus underestimated fraction of saturated area that contributes to overland flow during and after precipitation events. This is, however, not a general behaviour of the model as better comparison between measured and modelled specific discharge was observed at several other catchments (Fig. S2).

3.4 Within-catchment variability

3.4.1 Soil moisture

To illustrate how vegetation, soil and topography create within-catchment variability to local water fluxes and state variables, the relationship between $\langle \theta \rangle$ and its spatial standard deviation σ_θ at C3 Porkkavaara is shown in Fig. 8 for the two hydrologically contrasting years. Snapshots of spatial variability of θ and local saturation deficit of Topmodel (eq. 22) are further shown for dry and wet conditions in Fig. 9.

During winter, root zone moisture content decreases and its spatial variability is dampened by slow drainage. The onset of snowmelt is followed by infiltration peak and saturated soils nearly throughout the catchment (Fig. 7 – 9). This leads to rapid increase of σ_θ, mainly because of spatial variation in soil porosity. In wet 2012, drainage rapidly decreased σ_θ after snow melt, while the spatial variability was preserved until early July in the drier 2013. The latter result is because of spatially heterogeneous transpiration rate that created spatial variance of soil moisture and compensated for the dampening effect of drainage until ca. doy 180. After that σ_θ started to decrease because transpiration at grid cells characterized by coarse and medium-textured soil and high LAI (Fig. 3) become soil-moisture limited (eq. 7). In 2013 summer when $\langle\theta\rangle$ was most of the time well below field capacity, rainfall events tend to dampen spatial variability of soil moisture (Fig. 7). In wetter conditions (most of 2012, autumn 2013), however, the effect of infiltration is opposite and resembles that of spring snowmelt.

As a result, there is clear hysteresis of σ_θ with respect to antecedent $\langle\theta\rangle$ in the dry year while such patterns are less visible in moist conditions. This indicates soil and vegetation variability can in the model both create or destroy spatial variability of soil moisture, as has been proposed both by theoretical arguments (Albertson and Montaldo, 2003) and analysis of soil moisture observations (Teuling and Troch, 2005). To conclude, the role of landscape heterogeneity as driver of modelled soil moisture variability depends on antecedent soil moisture conditions and season; during drier spells variability is primarily driven by heterogeneous vegetation and plant water use, while soil type and topography become the primary controls in wet conditions and outside growing season (Seyfried and Wilcox, 1995; Teuling and Troch, 2005; Robinson et al., 2008).

3.4.2 ET and snow

Predicted spatial variability of evaporation fraction $\overline{ET/P}$ and its components are illustrated in Fig. 10. The model results, averaged over 2006 - 2016 period, reveal strong sensitivity of component ET fluxes to stand leaf area index, and secondary impacts of soil type and topography. The model predicts $\overline{ET/P}$ increases non-linearly with LAI and varies from >0.25 at grid cells where LAI < 1 $\mathrm{m^2 m^{-2}}$ to ∼0.65 at locations where the standing tree volume and LAI (Fig. 3) are largest. The shape of LAI-response results from the non-linear scaling of component fluxes with LAI, which also explain the inflection point at LAI ∼3 $\mathrm{m^2 m^{-2}}$.

Interception of rainfall and snow contributes from less than 5 to 30 % of long-term P, which is in line with measurements from boreal forests (Barbier et al., 2009; Toba and Ohta, 2005). The linear scaling of interception capacity with LAI and asymptotic approach of full storage (eq. 13), and temporal distribution of precipitation lead to the near-linear increase of $\overline{E/P}$ with increasing LAI (Fig. 10). At grid cells with high fraction of deciduous trees, low wintertime LAI leads to weaker snow interception and smaller annual $\overline{ET/P}$ compared to coniferous-dominated stands.

The model predictions suggest transpiration contributes from < 10 to more than 35 % of annual P being the largest ET component in stands whose LAI > 1.5 $\mathrm{m^2 m^{-2}}$ (Fig. 10). The shape of T_r to LAI -response is to most extent caused by saturation of G_c because of light limitations in dense stands (eq. 4). The more liberal water use strategy of deciduous species ($g_{1,d} > g_{1,c}$, Table 1) is reflected as higher transpiration rate at grid cells where deciduous trees form a significant part of total LAI. Moreover, the lower envelope of points occur at grid cells corresponding to coarse-textured soils (Fig. 3), where drought limitations become most frequent. This is visible also in $\overline{ET/P}$ at LAI > 2 $\mathrm{m^2 m^{-2}}$.

Evaporation from forest floor $\overline{ET/P}$ decreases asymptotically with LAI, showing complementary relationship to T_r, as expected by decreased available energy in denser stands. The upper envelope curve corresponds to grid cells with high TWI and large tendency to be permanently saturated due returnflow from the hillslope. In these grid cells E_f is mainly determined by available energy; however, rapid drying of the forest floor in sparse stands between rainfall events decreases $\overline{E_f/P}$ and explain its less steep decrease with LAI at grid cells receiving less frequent or no returnflow (lower TWI).

The spatial pattern of maximum SWE (Fig. 11) indicate snow accumulation in the densest stands ($LAI > 7$ m^{2}m^{-2}) was ~ 75 % of that on open areas; the exact fraction was found sensitive to winter weather conditions being lowest during mild winters in the southern catchments, and in years with smaller annual snowfall. The predicted impact of forest canopy on snow accumulation is in good agreement with observational studies from similar climatic conditions in Finland and Sweden (Koivusalo and Kokkonen, 2002; Lundberg and Koivusalo, 2003), although also higher snow interception losses have been reported (see Kozii et al. (2017) for summary). The near linear increase of snow interception and resulting decrease of SWE with LAI is supported by Hedstrom and Pomeroy (1998); Pomeroy et al. (2002).

4 Discussion

4.1 Modeling ET at stand and catchment scales

At stand-scale, SpaFHy was shown to well reproduce daily ET measured by eddy-covariance technique at several forest and peatland sites in Finland and Sweden (Fig. 4 and 5). The good performance using the generic parametrization derived mainly from literature sources and process-specific data suggests the model is capable of accounting for the key drivers of temporal and site-to-site variability of ET. The sensitivity analysis reveals that for given meteorological forcing, total LAI is the primary parameter affecting ET and its partitioning into component fluxes. In case of transpiration, the dominant role of LAI and parameters defining leaf water use efficiency (g_1 and A_{max}), and insensitivity to parameters related to aerodynamic conductance of the P-M equation (eq. 1) indicate variations in T_r are mainly governed by that of canopy conductance (eq. 4). The root zone depth, soil hydraulic properties and size of interception storage in the organic layer (z_{org} and $\theta_{fc,org}$) are important for the probability of drought occurrence and consequent reduction of transpiration (Table 4, Fig. 10). As rooting depths vary across species, site types and ecosystems (Gao et al., 2014) and soil heterogeneity is not fully represented by existing soil maps, uncertainties of these properties are large in general. It was, however, recently shown the root zone storage capacity can be estimated from satellite-based evaporation (Wang-Erlandsson et al., 2016), which may in future provide data to constrain these model parameters.

The multiplicative formulation for canopy conductance (eq. 4) was developed by coupling the commonly used unified stomatal model (Medlyn et al., 2012) and leaf-scale light response with simplified canopy radiative transfer scheme (see Suppl. S3). The approach accounts the non-linear scaling between G_c and g_s similarly as Saugier and Katerji (1991) and Kelliher et al. (1995). To derive bulk surface conductance for remote-sensing applications, Leuning et al. (2008) combined their G_c scheme with a ground evaporation model based on equilibrium evaporation (Priestley and Taylor, 1972). They showed that after site-specific optimization, the dry-canopy ET was accurately predicted by P-M equation across different vegetation types.

That particular model, however, still requires an arbitrary and non-measurable maximum g_s and few other parameters to be specified or calibrated. In our work g_s and its response to D were derived from stomatal optimization arguments and are tightly constrained by plant water use traits and photosynthetic capacity. These traits start to be widely available in databases such as TRY (Kattge et al., 2011), and can also be readily measured using leaf gas-exchange techniques. Due to these constraints on g_s, we consider eq. (4) as a major advancement of the Leuning et al. (2008) approach. The good comparison between modelled and measured dry-canopy ET for sites having strongly different T_r/ET and E_f/ET -ratios (Fig. 4 and 5) are indeed supportive for the proposed G_c formulation. However the comparison was done within a single vegetation type and further evaluation across ecosystem types are necessary to extend the approach outside boreal forests.

The sensitivity analysis (Table 4 and Fig. S1) proposes the P-M equation could be replaced with simpler approaches. Making the assumption that canopy is well-coupled to the atmosphere, reasonable for aerodynamically rough boreal forests, leads to $T_r = G_c \frac{D}{p_a}$, where p_a (Pa) is the ambient pressure. Also evaporation from the ground and canopy storage were found relatively insensitive to aerodynamic terms, which suggests these water fluxes could be computed proportional to equilibrium evaporation $E_i = \frac{\alpha_i}{L_v} \frac{\Delta R_{n,i}}{\Delta+\gamma}$, where α_i (-) is a proportionality factor calibrated against measurements, and $R_{n,i}$ available energy. Moving to such approaches would relax input data requirements by eliminating the canopy height and wind speed from model forcing.

Open GIS data on LAI, species composition, soil type and topography was used to apply SpaFHy at 16 x 16 m grid size to 21 headwater catchments in Finland. Results indicate the model well reproduces the variability of annual evaporation fraction across catchments (Fig. 6), as well as inter-annual variability at most of the studied catchments (not shown). It should be noted that the variability of annual $\left\langle \overline{ET/P} \right\rangle$ across the catchment space is dominated by the latitudinal climate gradient and further testing across different catchments on similar climatic conditions is needed.

Validation of spatial predictions of θ, ET or SWE (Fig. 9 – 11) was not attempted in this work. This would require either extensive spatially distributed and continuous *in situ* measurements, or high-resolution (i.e. order of tens of meters) remote sensing data that can be already obtained by near-ground microwave radiometry or low-frequency radars using unmanned aerial vehicles as a platform (Robinson et al., 2008). Also ongoing advances in satellite-based soil moisture (Chen et al., 2014) and ET products (Hu et al., 2015) could be used to evaluate the modelled spatial patterns and temporal evolution of these hydrological components.

The results of site and catchment scale validation suggest that ET and water budget partitioning in boreal forest-dominated landscape can be reasonably well predicted by the model based on generic parametrization, which is advantageous for scalability and applicability for areas and locations where data for model calibration is scarse or lacking. Moreover, the model-data comparison at catchment scale proposes ET components and water budgets can be upscaled from stand to catchment scale using relatively simple mechanistic approach that derives characteristics of the modelling domain from open GIS data.

4.2 Capabilities and limitations of the model framework

This study presented a semi-distributed model for boreal forest hydrology at stand and catchment scales (Fig. 1). The model consists of three independent components: a *Canopy* model for above-ground hydrology, a *Bucket* model for topsoil water balance and a *Topmodel* for point to catchment integration. The modularity of SpaFHy provides clear advantages since all

model components are independently parametrized which allows their stand-alone development and use, as well as inclusion to other distributed or lumped hydrological models. Moreover, parameters of each sub-model were obtained separately and calibrated based on good-quality data that clearly enhances the predictive power of SpaFHy by reasonably constraining the degree of freedom in model parametrization (Jakeman et al., 2006; Jackson-Blake et al., 2015).

In SpaFHy, the above-ground hydrology and root zone water balance (eq. 16 & 17) are solved distributively (Fig. 1), which propagates the spatial variability of vegetation (LAI, c_f, species composition) and soil type into the local hydrological fluxes, SWE and organic layer and root zone water contents. Applied stand-alone, such approach would assume grid cell water balances are independent from each other, and omits the role of lateral flows and topographic position of a grid cell on a hillslope. The role of *Topmodel* (sect. 2.3) can be considered as a non-linear streamflow generation routine, which delays average root zone drainage signal $\overline{D_r}$ leading to realistic response of streamflow to P as controlled by TWI distribution. The other catchment properties are lumped into the parameter m, the effective subsurface water-conducting depth. It is this parameter that primarily controls both the shape of rainfall-runoff response and streamflow recession. The SpaFHy can thus be used as a simple catchment model to predict the signals of vegetation changes, forest management or varying climatic drivers on streamflow at daily or longer time scales. Indeed, the daily time series of streamflow (Fig. 7 and Fig. S2) were well reproduced for majority of the 21 studied catchments although m was the only parameter specifically calibrated for each catchment (Suppl. Table 2).

On the other hand, SpaFHy can assist in mapping how soil saturation may vary spatially and temporally as response to weather forcing (Fig. 9). The TWI-based scaling in *Topmodel* is used to predict magnitude and location of returnflow formation based on state of the catchment sub-surface storage. The spatial Q_r field is then used to update *Bucket* sub-model water storages and θ at respective grid-cells. In this way, SpaFHy can be used to predict local soil saturation that depends on both local (via vegetation and soil characteristics) and approximative landscape (via topography) controls (Fig. 9). In essence, the effect of returnflow formation is to delay drying of gridcells that receive water from the surrounding landscape. Depending on TWI-distribution and value of m, this conceptualization implies that some gridcells never receive water from the surrounding landscape(those with low TWI) while some receive Q_r in highflow conditions but not in baseflow conditions. At the other extreme, there are permanently inundated areas (high TWI) that contribute constantly to overland flow.

We emphasize that linking grid-cell water balances through *Topmodel* is conceptual rather than physically correct approach (Beven, 1997; Seibert et al., 1997; Kirkby, 1997), and driven by the goal to develop a simple and practically applicable representation of topographic controls of soil moisture. Future work should explore whether m can be related to catchment characteristics to derive a more generic parametrization for *Topmodel*, as well as analyse the impact of parameter uncertainty on streamflow and saturated area predictions. For applications requiring more rigorous treatment of sub-surface flows, the *Topmodel* can be replaced with 2D ground water flow schemes.

Fig. 9 and 10 show that landscape position (accounted via TWI) can markedly affect grid cell soil moisture and ET. In this work, other topographic controls were omitted for simplicity. While likely to have small impact for annual catchment water balance, including topographic effects on radiation (Dubayah and Rich, 1995) is presumed to alter the spatial patterns of ET and θ. In addition, the shading by vegetation at the neighbouring grid cells should be considered to derive a more comprehensive

understanding on landscape level hydrological variability. Also adding sub-models to simulate spatial and temporal patterns of soil temperature and frost depth, vegetation productivity and carbon balance would be relatively straightforward future developments.

As shown in this work, the mNFI data (Mäkisara et al., 2016) can provide estimates of LAI, canopy height, site type and conifer/deciduous composition at 16 x 16m resolution throughout Finland. Härkönen et al. (2015) compared mNFI-based LAI estimates against ground-based estimates and MODIS AI, and found good agreement between the methods. Consequently, the mNFI data can provide an easy way to obtain vegetation characteristics for hydrological and biogeochemical models at spatial scale currently unresolved by e.g. MODIS and other satellite products. Similar high-resolution data on forest resources is openly available also from the other Nordic countries (Kangas et al., 2018).

4.3 Potential applications

The proposed modular framework can provide support to a variety of questions benefiting from spatial and temporal hydrological predictions. These include, but are not limited to: (1) predicting soil moisture necessary for forecasting forest soil trafficability (Vega-Nieva et al., 2009; Jones and Arp, 2017), precision forestry, and confronting climate-induced risks (Muukkonen et al., 2015); (2) identifying how saturated areas, considered as biogeochemical and biodiversity hotspots particularly sensitive to negative environmental impacts of human activities, evolve in time (Laudon et al., 2016; Ågren et al., 2015); (3) addressing impacts of forest structure, management and climate change on ET partitioning, streamflow dynamics and soil moisture (Zhang et al., 2017; Karlsen et al., 2016); (4) supporting water-quality modelling in headwater catchments (Guan et al., 2018); and (5) providing starting point for developing spatially distributed forest productivity and sustainability framework that combines open data streams, statistical approaches and mechanistic models. Moreover, we propose the *Canopy* sub-model, in particular the leaf-to-canopy upscaling of canopy conductance, to be tested more widely in other ecosystems.

5 Conclusions

A distributed hydrological model framework for predicting ET and other hydrological processes from a grid cell to catchment level using open GIS-data and daily meteorological data was presented and validated for boreal coniferous-dominated forests and peatlands. SpaFHy consists of coupled, stand-alone modules for aboveground, topsoil and subsurface domains. An improved approach to upscale stomatal conductance to canopy scale was proposed, and a generic parametrization of vegetation and snow-related hydrological processes for Nordic boreal forest and peatland ecosystems derived. With the generic parametrization, daily ET was well reproduced across conifer-dominated forest stands whose LAI ranged from 0.2 to 6.8 $\mathrm{m^2 m^{-2}}$. Predictions of annual ET were successful for the considered 21 boreal headwater catchments in Finland located from 60 to 68 °N, and daily specific discharge could be reasonably well predicted for majority of the catchments by calibrating only one parameter against streamflow data. In subsequent studies, the model will be used to support forest trafficability forecasting, and predicting the impacts of climate change and forest management on stand and catchment water balance.

Code and data availability. The SpaFHy source code (Python 2.7/3.6), a brief user manual and a sample dataset to run the model for a single forest stand and for a single catchment are available under MIT license at www.github.com/lukeecomod/spafhy_v1. Data from a Hyytiälä (FIHy) used in stand-scale evaluation is available at https://avaa.tdata.fi/web/avaa/-/smartsmear. Eddy-covariance data from other sites, and the specific discharge data used in Topmodel calibration and catchment scale evaluation can be obtained from the corresponding author. All GIS-data used in this work is openly available for whole Finland; the entry-point for obtaining GIS-data in Finland is https://www.paikkatietoikkuna.fi/?lang=en. The mNFI -data at 16 m resolution is available at http://kartta.luke.fi/index-en.html.

Author contributions. SL conceived and designed the study and was the main developer of the model. MG and AK contributed to model design, simulations, calibration and sensitivity analysis and AS processed the GIS-data for the catchment simulations. The authors jointly analysed and interpreted the results and wrote the paper.

Competing interests. The authors declare that they have no conflict of interest.

Acknowledgements. This study was financially supported through the following projects: the Academy of Finland CLIMOSS (no. 296116 & 307192) and FOTETRAF (no. 295337); Swedish Research Council for Environment, Agricultural Sciences and Spatial Planning (FORMAS, grant no. 2018-01820) and EU Life+ FRESHHABIT. We acknowledge University of Lund (sites SENor, SEKno, SESky2) and University of Helsinki (FIHy, FICage, FISii) for providing the eddy-covariance data for model validation. The Finnish Meteorological Institute is acknowledged for providing the eddy-covariance data (FISod, FIKal, FILet) and 10x10 km weather data. The catchment monitoring network used in this work is funded by the Ministry of Agriculture and Forestry of Finland.

References

Ågren, A. M., Lidberg, W., and Ring, E.: Mapping temporal dynamics in a forest stream network—implications for riparian forest management, Forests, 6, 2982–3001, 2015.

Ala-aho, P., Tetzlaff, D., McNamara, J. P., Laudon, H., and Soulsby, C.: Using isotopes to constrain water flux and age estimates in snow-influenced catchments using the STARR (Spatially distributed Tracer-Aided Rainfall–Runoff) model, Hydrology and Earth System Sciences, 21, 5089–5110, https://doi.org/10.5194/hess-21-5089-2017, https://www.hydrol-earth-syst-sci.net/21/5089/2017/, 2017.

Albertson, J. D. and Montaldo, N.: Temporal dynamics of soil moisture variability: 1. Theoretical basis, Water Resources Research, 39, 2003.

Alekseychik, P., Korrensalo, A., Mammarella, I., Vesala, T., and Tuittila, E.-S.: Relationship between aerodynamic roughness length and bulk sedge leaf area index in a mixed-species boreal mire complex, Geophysical Research Letters, 44, 5836–5843, 2017.

Allen, R. G., Pereira, L. S., Raes, D., Smith, M., et al.: Crop evapotranspiration-Guidelines for computing crop water requirements-FAO Irrigation and drainage paper 56, Fao, Rome, 300, D05 109, 1998.

Aston, A.: Rainfall interception by eight small trees, Journal of Hydrology, 42, 383–396, 1979.

Aurela, M.: Carbon dioxide exchange in subarctic ecosystems measured by a micrometeorological technique, Ph.D. thesis, Finnish Meteorological Institute, http://ethesis.helsinki.fi/julkaisut/mat/fysik/vk/aurela/carbondi.pdf, 2005.

Barbier, S., Balandier, P., and Gosselin, F.: Influence of several tree traits on rainfall partitioning in temperate and boreal forests: a review, Annals of Forest Science, 66, 1–11, 2009.

Berggren, D., Bergkvist, B., Johansson, M.-B., Langvall, O., Majdi, H., Melkerud, P.-A., Nilsson, Å., Weslien, P., and Olsson, M.: A description of LUSTRA's common field sites, vol. 87, Swedish University of Agricultural Sciences, 2004.

Bergström, S.: The HBV model: Its structure and applications, no. 4 in SMHI Reports Hydrology, Swedish Meteorological and Hydrological Institute, 1992.

Best, M., Pryor, M., Clark, D., Rooney, G., Essery, R., Ménard, C., Edwards, J., Hendry, M., Porson, A., Gedney, N., et al.: The Joint UK Land Environment Simulator (JULES), model description–Part 1: energy and water fluxes, Geoscientific Model Development, 4, 677–699, 2011.

Beven, K.: TOPMODEL: a critique, Hydrological processes, 11, 1069–1085, 1997.

Beven, K. and Kirkby, M. J.: A physically based, variable contributing area model of basin hydrology/Un modèle à base physique de zone d'appel variable de l'hydrologie du bassin versant, Hydrological Sciences Journal, 24, 43–69, 1979.

Bonan, G., Williams, M., Fisher, R., and Oleson, K.: Modeling stomatal conductance in the earth system: linking leaf water-use efficiency and water transport along the soil–plant–atmosphere continuum, Geoscientific Model Development, 7, 2193–2222, 2014.

Bonan, G. B.: Forests and climate change: Forcings, feedbacks, and the climate benefits of forests, Science, 320, 1444–1449, 2008.

Campbell, G. S.: Soil Physics with BASIC: Transport Models for Soil-Plant Systems, Elsevier, 1st edn., 1985.

Campolongo, F., Cariboni, J., and Saltelli, A.: An effective screening design for sensitivity analysis of large models, Environmental Modelling & Software, 22, 1509–1518, 2007.

Chapin, F., McGuire, A., Randerson, J., Pielke, R., Baldocchi, D., Hobbie, S., Roulet, N., Eugster, W., Kasischke, E., Rastetter, E., et al.: Arctic and boreal ecosystems of western North America as components of the climate system, Global Change Biology, 6, 211–223, 2000.

Chen, T., De Jeu, R., Liu, Y., Van der Werf, G., and Dolman, A.: Using satellite based soil moisture to quantify the water driven variability in NDVI: A case study over mainland Australia, Remote Sensing of Environment, 140, 330–338, 2014.

Clark, M. P., Kavetski, D., and Fenicia, F.: Pursuing the method of multiple working hypotheses for hydrological modeling, Water Resources Research, 47, 2011.

Clark, M. P., Nijssen, B., Lundquist, J. D., Kavetski, D., Rupp, D. E., Woods, R. A., Freer, J. E., Gutmann, E. D., Wood, A. W., Brekke, L. D., et al.: A unified approach for process-based hydrologic modeling: 1. Modeling concept, Water Resources Research, 51, 2498–2514, 2015a.

Clark, M. P., Nijssen, B., Lundquist, J. D., Kavetski, D., Rupp, D. E., Woods, R. A., Freer, J. E., Gutmann, E. D., Wood, A. W., Gochis, D. J., et al.: A unified approach for process-based hydrologic modeling: 2. Model implementation and case studies, Water Resources Research, 51, 2515–2542, 2015b.

Cowan, I. and Farquhar, G.: Stomatal function in relation to leaf metabolism and environment., in: Symposia of the Society for Experimental Biology, vol. 31, p. 471, 1977.

Dubayah, R. and Rich, P. M.: Topographic solar radiation models for GIS, International Journal of Geographical Information Systems, 9, 405–419, 1995.

Essery, R., Pomeroy, J., Parviainen, J., and Storck, P.: Sublimation of snow from coniferous forests in a climate model, Journal of Climate, 16, 1855–1864, 2003.

Ferone, J. and Devito, K.: Shallow groundwater–surface water interactions in pond–peatland complexes along a Boreal Plains topographic gradient, Journal of Hydrology, 292, 75–95, 2004.

Finér, L., Piirainen, S., Launiainen, S., Laurén, A., Mattsson, T., Tattari, S., Linjama, J., et al.: Metsätalouden vesistökuormituksen seuranta-ja raportointiohjelma, Luonnonvara- ja biotalouden tutkimus, http://urn.fi/URN:ISBN:978-952-326-388-8, 2017.

Fisher, J. B., DeBiase, T. A., Qi, Y., Xu, M., and Goldstein, A. H.: Evapotranspiration models compared on a Sierra Nevada forest ecosystem, Environmental Modelling & Software, 20, 783–796, 2005.

Freeze, R. A. and Harlan, R.: Blueprint for a physically-based, digitally-simulated hydrologic response model, Journal of Hydrology, 9, 237–258, 1969.

Gao, H., Hrachowitz, M., Fenicia, F., Gharari, S., and Savenije, H.: Testing the realism of a topography driven model (FLEX-Topo) in the nested catchments of the Upper Heihe, China., Hydrology & Earth System Sciences Discussions, 10, 2013.

Gao, H., Hrachowitz, M., Schymanski, S., Fenicia, F., Sriwongsitanon, N., and Savenije, H.: Climate controls how ecosystems size the root zone storage capacity at catchment scale, Geophysical Research Letters, 41, 7916–7923, 2014.

Gauthier, S., Bernier, P., Kuuluvainen, T., Shvidenko, A., and Schepaschenko, D.: Boreal forest health and global change, Science, 349, 819–822, 2015.

Gioli, B., Miglietta, F., De Martino, B., Hutjes, R. W., Dolman, H. A., Lindroth, A., Schumacher, M., Sanz, M. J., Manca, G., Peressotti, A., et al.: Comparison between tower and aircraft-based eddy covariance fluxes in five European regions, Agricultural and Forest Meteorology, 127, 1–16, 2004.

Govind, A., Chen, J. M., Bernier, P., Margolis, H., Guindon, L., and Beaudoin, A.: Spatially distributed modeling of the long-term carbon balance of a boreal landscape, Ecological Modelling, 222, 2780–2795, 2011.

Grayson, R. B., Moore, I. D., and McMahon, T. A.: Physically based hydrologic modeling: 1. A terrain-based model for investigative purposes, Water Resources Research, 28, 2639–2658, 1992.

GSF: Geological Survey of Finland, bedrock 1:200 000 and superficial deposits 1:20 000 and 1:50 000, https://hakku.gtk.fi/en, 2015.

Guan, M., Laurén, A., Launiainen, S., and Salmivaara, A.: Modelling water and nutrient dynamics in boreal forested catchments: evaluation and application of a distributed model, in: EGU General Assembly Conference Abstracts, vol. 20, p. 16025, 2018.

Hari, P. and Kulmala, M.: Station for measuring ecosystem-atmosphere relations (SMEAR II), Boreal Environment Research, 10, 315–322, 2005.

Härkönen, S., Lehtonen, A., Manninen, T., Tuominen, S., Peltoniemi, M., et al.: Estimating forest leaf area index using satellite images: comparison of k-NN based Landsat-NFI LAI with MODIS-RSR based LAI product for Finland, Boreal Environment Research, 20, 181–195, 2015.

Hedstrom, N. and Pomeroy, J.: Measurements and modelling of snow interception in the boreal forest, Hydrological Processes, 12, 1611–1625, 1998.

Herman, J. and Usher, W.: SALib: an open-source Python library for sensitivity analysis, The Journal of Open Source Software, 2, https://doi.org/10.21105/joss.00097, 2017.

Herman, M. R., Nejadhashemi, A. P., Abouali, M., Hernandez-Suarez, J. S., Daneshvar, F., Zhang, Z., Anderson, M. C., Sadeghi, A. M., Hain, C. R., and Sharifi, A.: Evaluating the role of evapotranspiration remote sensing data in improving hydrological modeling predictability, Journal of Hydrology, 556, 39–49, 2018.

Hu, G., Jia, L., and Menenti, M.: Comparison of MOD16 and LSA-SAF MSG evapotranspiration products over Europe for 2011, Remote Sensing of Environment, 156, 510–526, 2015.

Ilvesniemi, H., Pumpanen, J., Duursma, R., Hari, P., Keronen, P., Kolari, P., Kulmala, M., Mammarella, I., Nikinmaa, E., Rannik, Ü., et al.: Water balance of a boreal Scots pine forest., Boreal Environment Research, 15, 2010.

Ivanov, V. Y., Vivoni, E. R., Bras, R. L., and Entekhabi, D.: Catchment hydrologic response with a fully distributed triangulated irregular network model, Water Resources Research, 40, 2004.

Jackson-Blake, L. A., Dunn, S., Helliwell, R., Skeffington, R., Stutter, M., and Wade, A. J.: How well can we model stream phosphorus concentrations in agricultural catchments?, Environmental Modelling & Software, 64, 31–46, 2015.

Jakeman, A. J., Letcher, R. A., and Norton, J. P.: Ten iterative steps in development and evaluation of environmental models, Environmental Modelling & Software, 21, 602–614, 2006.

Jones, M.-F. and Arp, P. A.: Relating cone penetration and rutting resistance to variations in forest soil properties and daily moisture fluctuations, Open J Soil Sci, 7, 149–171, 2017.

Kalliokoski, T., Pennanen, T., Nygren, P., Sievänen, R., and Helmisaari, H.-S.: Belowground interspecific competition in mixed boreal forests: fine root and ectomycorrhiza characteristics along stand developmental stage and soil fertility gradients, Plant and Soil, 330, 73–89, 2010.

Kang, M., Kim, J., Malla Thakuri, B., Chun, J., and Cho, C.: New gap-filling and partitioning technique for H2O eddy fluxes measured over forests, Biogeosciences, 15, 631–647, 2018.

Kangas, A., Astrup, R., Breidenbach, J., Fridman, J., Gobakken, T., Korhonen, K. T., Maltamo, M., Nilsson, M., Nord-Larsen, T., Næsset, E., et al.: Remote sensing and forest inventories in Nordic countries–roadmap for the future, Scandinavian Journal of Forest Research, 33, 397–412, 2018.

Karlsen, R. H., Grabs, T., Bishop, K., Buffam, I., Laudon, H., and Seibert, J.: Landscape controls on spatiotemporal discharge variability in a boreal catchment, Water Resources Research, 52, 6541–6556, 2016.

Kattge, J., Diaz, S., Lavorel, S., Prentice, I. C., Leadley, P., Bönisch, G., Garnier, E., Westoby, M., Reich, P. B., Wright, I. J., et al.: TRY–a global database of plant traits, Global Change biology, 17, 2905–2935, 2011.

Katul, G. G., Oren, R., Manzoni, S., Higgins, C., and Parlange, M. B.: Evapotranspiration: a process driving mass transport and energy exchange in the soil-plant-atmosphere-climate system, Reviews of Geophysics, 50, 2012.

Kelliher, F., Leuning, R., Raupach, M., and Schulze, E.-D.: Maximum conductances for evaporation from global vegetation types, Agricultural and Forest Meteorology, 73, 1–16, 1995.

Khakbaz, B., Imam, B., Hsu, K., and Sorooshian, S.: From lumped to distributed via semi-distributed: Calibration strategies for semi-distributed hydrologic models, Journal of Hydrology, 418, 61–77, 2012.

Kirkby, M.: TOPMODEL: A personal view, Hydrological Processes, 11, 1087–1097, 1997.

Koivusalo, H. and Kokkonen, T.: Snow processes in a forest clearing and in a coniferous forest, Journal of Hydrology, 262, 145–164, 2002.

Kolari, P., Pumpanen, J., Rannik, Ü., Ilvesniemi, H., Hari, P., and Berninger, F.: Carbon balance of different aged Scots pine forests in Southern Finland, Global Change Biology, 10, 1106–1119, 2004.

Kolari, P., Lappalainen, H. K., Hänninen, H., and Hari, P.: Relationship between temperature and the seasonal course of photosynthesis in Scots pine at northern timberline and in southern boreal zone, Tellus B, 59, 542–552, 2007a.

Kolari, P., Lappalainen, H. K., Hänninen, H., and Hari, P.: Relationship between temperature and the seasonal course of photosynthesis in Scots pine at northern timberline and in southern boreal zone, Tellus Series B-Chemical and Physical Meteorology, 59, 542–552, 2007b.

Koskinen, M., Minkkinen, K., Ojanen, P., Kämäräinen, M., Laurila, T., and Lohila, A.: Measurements of CO_2 exchange with an automated chamber system throughout the year: challenges in measuring night-time respiration on porous peat soil, Biogeosciences, 11, 347–363, 2014.

Kozii, N., Laudon, H., Ottosson-Löfvenius, M., and Hasselquist, N. J.: Increasing water losses from snow captured in the canopy of boreal forests: A case study using a 30 year data set, Hydrological Processes, 31, 3558–3567, 2017.

Krause, P., Boyle, D., and Bäse, F.: Comparison of different efficiency criteria for hydrological model assessment, Advances in Geosciences, 5, 89–97, 2005.

Kuusisto, E.: Snow accumulation and snowmelt in Finland, vol. 55, Valtion painatuskeskus, Finland, 1984.

Lagergren, F. and Lindroth, A.: Transpiration response to soil moisture in pine and spruce trees in Sweden, Agricultural and Forest Meteorology, 112, 67–85, 2002.

Laudon, H., Kuglerová, L., Sponseller, R. A., Futter, M., Nordin, A., Bishop, K., Lundmark, T., Egnell, G., and Ågren, A. M.: The role of biogeochemical hotspots, landscape heterogeneity, and hydrological connectivity for minimizing forestry effects on water quality, Ambio, 45, 152, 2016.

Launiainen, S., Katul, G. G., Lauren, A., and Kolari, P.: Coupling boreal forest CO2, H2O and energy flows by a vertically structured forest canopy – Soil model with separate bryophyte layer, Ecological Modelling, 312, 385–405, 2015.

Launiainen, S., Katul, G. G., Kolari, P., Lindroth, A., Lohila, A., Aurela, M., Varlagin, A., Grelle, A., and Vesala, T.: Do the energy fluxes and surface conductance of boreal coniferous forests in Europe scale with leaf area?, Global Change Biology, 22, 4096–4113, 2016.

Laurén, A. and Heiskanen, J.: Physical properties of the mor layer in a Scots pine stand I. Hydraulic conductivity, Canadian journal of soil science, 77, 627–634, 1997.

Leuning, R., Zhang, Y. Q., Rajaud, A., Cleugh, H., and Tu, K.: A simple surface conductance model to estimate regional evaporation using MODIS leaf area index and the Penman-Monteith equation, Water Resources Research, 44, https://doi.org/10.1029/2007WR006562, http://dx.doi.org/10.1029/2007WR006562, w10419, 2008.

Lin, Y.-S., Medlyn, B. E., Duursma, R. A., Prentice, I. C., Wang, H., Baig, S., Eamus, D., de Dios, V. R., Mitchell, P., Ellsworth, D. S., et al.: Optimal stomatal behaviour around the world, Nature Climate Change, 5, 459, 2015.

Lindroth, A., Klemedtsson, L., Grelle, A., Weslien, P., and Langvall, O.: Measurement of net ecosystem exchange, productivity and respiration in three spruce forests in Sweden shows unexpectedly large soil carbon losses, Biogeochemistry, 89, 43–60, 2008.

Lindsay, J.: The whitebox geospatial analysis tools project and open-access GIS, in: Proceedings of the GIS Research UK 22nd Annual Conference, The University of Glasgow, pp. 16–18, 2014.

Lindsay, J. B.: The practice of DEM stream burning revisited, Earth Surface Processes and Landforms, 41, 658–668, 2016.

Linkosalo, T., Heikkinen, J., Pulkkinen, P., and Mäkipää, R.: Fluorescence measurements show stronger cold inhibition of photosynthetic light reactions in Scots pine compared to Norway spruce as well as during spring compared to autumn, Frontiers in Plant Science, 5, 264, 2014.

Lohila, A., Minkkinen, K., Aurela, M., Tuovinen, J.-P., Penttilä, T., Ojanen, P., and Laurila, T.: Greenhouse gas flux measurements in a forestry-drained peatland indicate a large carbon sink, Biogeosciences, 8, 3203–3218, 2011.

Lundberg, A. and Koivusalo, H.: Estimating winter evaporation in boreal forests with operational snow course data, Hydrological Processes, 17, 1479–1493, 2003.

Lundin, L.-C., Halldin, S., Lindroth, A., et al.: Continuous long-term measurements of soil-plant-atmosphere variables at a forest site, Agricultural and Forest Meteorology, 98, 53–73, 1999.

Ma, L., He, C., Bian, H., and Sheng, L.: MIKE SHE modeling of ecohydrological processes: Merits, applications, and challenges, Ecological Engineering, 96, 137–149, 2016.

Magnani, F., Leonardi, S., Tognetti, R., Grace, J., and Borghetti, M.: Modelling the surface conductance of a broad-leaf canopy: effects of partial decoupling from the atmosphere, Plant, Cell & Environment, 21, 867–879, 1998.

Mäkisara, K., Katila, M., Peräsaari, J., Tomppo, E., et al.: The Multi-Source National Forest Inventory of Finland–methods and results 2013, Natural resources and bioeconomy studies, http://urn.fi/URN:ISBN:978-952-326-186-0, 2016.

McDonnell, J., Sivapalan, M., Vaché, K., Dunn, S., Grant, G., Haggerty, R., Hinz, C., Hooper, R., Kirchner, J., Roderick, M., et al.: Moving beyond heterogeneity and process complexity: A new vision for watershed hydrology, Water Resources Research, 43, 2007.

McGuire, A., Wirth, C., Apps, M., Beringer, J., Clein, J., Epstein, H., Kicklighter, D., Bhatti, J., Chapin III, F., De Groot, B., et al.: Environmental variation, vegetation distribution, carbon dynamics and water/energy exchange at high latitudes, Journal of Vegetation Science, 13, 301–314, 2002.

Medlyn, B. E., Duursma, R. A., Eamus, D., et al.: Reconciling the optimal and empirical approaches to modelling stomatal conductance, Global Change Biology, 18, 3476–3476, 2012.

Mendoza, M., Bocco, G., and Bravo, M.: Spatial prediction in hydrology: status and implications in the estimation of hydrological processes for applied research, Progress in Physical Geography, 26, 319–338, 2002.

Minunno, F., Peltoniemi, M., Launiainen, S., Aurela, M., Lindroth, A., Lohila, A., Mammarella, I., Minkkinen, K., and Mäkelä, A.: Calibration and validation of a semi-empirical flux ecosystem model for coniferous forests in the boreal region, Ecological Modelling, 341, 37–52, 2016.

Montanari, A. and Koutsoyiannis, D.: A blueprint for process-based modeling of uncertain hydrological systems, Water Resources Research, 48, 2012.

Monteith, J. and Unsworth, M.: Principles of Environmental Physics, Academic press, 3rd edn., 2008.

Morris, M. D.: Factorial sampling plans for preliminary computational experiments, Technometrics, 33, 161–174, 1991.

Muukkonen, P., Nevalainen, S., Lindgren, M., Peltoniemi, M., et al.: Spatial occurrence of drought-associated damages in Finnish boreal forests: results from forest condition monitoring and GIS analysis, Boreal Environmental Research, 20, 172–180, 2015.

Niu, G.-Y., Yang, Z.-L., Mitchell, K. E., Chen, F., Ek, M. B., Barlage, M., Kumar, A., Manning, K., Niyogi, D., Rosero, E., et al.: The community Noah land surface model with multiparameterization options (Noah-MP): 1. Model description and evaluation with local-scale measurements, Journal of Geophysical Research: Atmospheres, 116, 2011.

NSLF: National Land Survey of Finland Topographic Database., http://www.maanmittauslaitos.fi/en/e-services/open-data-file-download-service, 2017.

Panday, S. and Huyakorn, P. S.: A fully coupled physically-based spatially-distributed model for evaluating surface/subsurface flow, Advances in Water Resources, 27, 361–382, 2004.

Pomeroy, J., Parviainen, J., Hedstrom, N., and Gray, D.: Coupled modelling of forest snow interception and sublimation, Hydrological Processes, 12, 2317–2337, 1998.

Pomeroy, J., Gray, D., Hedstrom, N., and Janowicz, J.: Prediction of seasonal snow accumulation in cold climate forests, Hydrological Processes, 16, 3543–3558, 2002.

Price, D. T., Alfaro, R., Brown, K., Flannigan, M., Fleming, R., Hogg, E., Girardin, M., Lakusta, T., Johnston, M., McKenney, D., et al.: Anticipating the consequences of climate change for Canada's boreal forest ecosystems, Environmental Reviews, 21, 322–365, 2013.

Priestley, C. and Taylor, R.: On the assessment of surface heat flux and evaporation using large-scale parameters, Monthly Weather Review, 100, 81–92, 1972.

Rannik, Ü., Altimir, N., Raittila, J., et al.: Fluxes of carbon dioxide and water vapour over Scots pine forest and clearing, Agricultural and Forest Meteorology, 111, 187–202, 2002.

Reed, S., Koren, V., Smith, M., Zhang, Z., Moreda, F., Seo, D.-J., and Participants, D.: Overall distributed model intercomparison project results, Journal of Hydrology, 298, 27–60, 2004.

Robinson, D., Campbell, C., Hopmans, J., Hornbuckle, B. K., Jones, S. B., Knight, R., Ogden, F., Selker, J., and Wendroth, O.: Soil moisture measurement for ecological and hydrological watershed-scale observatories: A review, Vadose Zone Journal, 7, 358–389, 2008.

Rouse, W. R.: A water balance model for a subarctic sedge fen and its application to climatic change, Climatic change, 38, 207–234, 1998.

Ruano, M., Ribes, J., Ferrer, J., and Sin, G.: Application of the Morris method for screening the influential parameters of fuzzy controllers applied to wastewater treatment plants, Water Science and Technology, 63, 2199–2206, 2011.

Ruano, M., Ribes, J., Seco, A., and Ferrer, J.: An improved sampling strategy based on trajectory design for application of the Morris method to systems with many input factors, Environmental Modelling & Software, 37, 103–109, 2012.

Ryu, Y., Baldocchi, D. D., Kobayashi, H., van Ingen, C., Li, J., Black, T. A., Beringer, J., Van Gorsel, E., Knohl, A., Law, B. E., et al.: Integration of MODIS land and atmosphere products with a coupled-process model to estimate gross primary productivity and evapotranspiration from 1 km to global scales, Global Biogeochemical Cycles, 25, 2011.

Samaniego, L., Kumar, R., and Attinger, S.: Multiscale parameter regionalization of a grid-based hydrologic model at the mesoscale, Water Resources Research, 46, 2010.

Saugier, B. and Katerji, N.: Some plant factors controlling evapotranspiration, Agricultural and Forest Meteorology, 54, 263–277, 1991.

Savenije, H.: HESS Opinions" Topography driven conceptual modelling (FLEX-Topo)", Hydrology and Earth System Sciences, 14, 2681–2692, 2010.

Seibert, J., Bishop, K. H., and Nyberg, L.: A test of TOPMODEL'a ability to predict spatially distributed groundwater levels, Hydrological Processes, 11, 1131–1144, 1997.

Seyfried, M. S. and Wilcox, B.: Scale and the nature of spatial variability: Field examples having implications for hydrologic modeling, Water Resources Research, 31, 173–184, 1995.

Sperry, J. S.: Hydraulic constraints on plant gas exchange, Agricultural and Forest meteorology, 104, 13–23, 2000.

Spittlehouse, D. L.: Integrating climate change adaptation into forest management, The Forestry Chronicle, 81, 691–695, 2005.

Stoy, P. C., Mauder, M., Foken, T., Marcolla, B., Boegh, E., Ibrom, A., Arain, M. A., Arneth, A., Aurela, M., Bernhofer, C., et al.: A data-driven analysis of energy balance closure across FLUXNET research sites: The role of landscape scale heterogeneity, Agricultural and forest meteorology, 171, 137–152, 2013.

Tarboton, D. G.: A new method for the determination of flow directions and upslope areas in grid digital elevation models, Water Resources Research, 33, 309–319, 1997.

Teuling, A. J. and Troch, P. A.: Improved understanding of soil moisture variability dynamics, Geophysical Research Letters, 32, 2005.

Thum, T., Aalto, T., Laurila, T., Aurela, M., Kolari, P., and Hari, P.: Parametrization of two photosynthesis models at the canopy scale in a northern boreal Scots pine forest, Tellus B, 59, 874–890, 2007.

Toba, T. and Ohta, T.: An observational study of the factors that influence interception loss in boreal and temperate forests, Journal of Hydrology, 313, 208–220, 2005.

Tyree, M. T. and Zimmermann, M. H.: Hydraulic architecture of whole plants and plant performance, in: Xylem structure and the ascent of sap, pp. 175–214, Springer, 2002.

van Dijk, A. I., Gash, J. H., van Gorsel, E., Blanken, P. D., Cescatti, A., Emmel, C., Gielen, B., Harman, I. N., Kiely, G., Merbold, L., et al.: Rainfall interception and the coupled surface water and energy balance, Agricultural and Forest meteorology, 214, 402–415, 2015.

Vega-Nieva, D. J., Murphy, P. N., Castonguay, M., Ogilvie, J., and Arp, P. A.: A modular terrain model for daily variations in machine-specific forest soil trafficability, Canadian Journal of Soil Science, 89, 93–109, 2009.

Vivoni, E. R., Mascaro, G., Mniszewski, S., Fasel, P., Springer, E. P., Ivanov, V. Y., and Bras, R. L.: Real-world hydrologic assessment of a fully-distributed hydrological model in a parallel computing environment, Journal of Hydrology, 409, 483–496, 2011.

Wagener, T., Boyle, D. P., Lees, M. J., Wheater, H. S., Gupta, H. V., and Sorooshian, S.: A framework for development and application of hydrological models, Hydrology and Earth System Sciences, 5, 13–26, 2001.

Wang-Erlandsson, L., Bastiaanssen, W. G., Gao, H., Jagermeyr, J., Senay, G. B., Van Dijk, A., Guerschman, J. P., Keys, P. W., Gordon, L. J., Savenije, H. H., et al.: Global root zone storage capacity from satellite-based evaporation, 2016.

Williams, C. A., Reichstein, M., Buchmann, N., Baldocchi, D., Beer, C., Schwalm, C., Wohlfahrt, G., Hasler, N., Bernhofer, C., Foken, T., et al.: Climate and vegetation controls on the surface water balance: Synthesis of evapotranspiration measured across a global network of flux towers, Water Resources Research, 48, 2012.

Williams, T. G. and Flanagan, L. B.: Effect of changes in water content on photosynthesis, transpiration and discrimination against 13 CO 2 and C 18 O 16 O in Pleurozium and Sphagnum, Oecologia, 108, 38–46, 1996.

Zeng, Z., Piao, S., Li, L. Z., Wang, T., Ciais, P., Lian, X., Yang, Y., Mao, J., Shi, X., and Myneni, R. B.: Impact of Earth greening on the terrestrial water cycle, Journal of Climate, 31, 2633–2650, 2018.

Zhang, M., Liu, N., Harper, R., Li, Q., Liu, K., Wei, X., Ning, D., Hou, Y., and Liu, S.: A global review on hydrological responses to forest change across multiple spatial scales: Importance of scale, climate, forest type and hydrological regime, Journal of Hydrology, 546, 44–59, 2017.

Zhao, L., Xia, J., Xu, C.-y., Wang, Z., Sobkowiak, L., and Long, C.: Evapotranspiration estimation methods in hydrological models, Journal of Geographical Sciences, 23, 359–369, 2013.

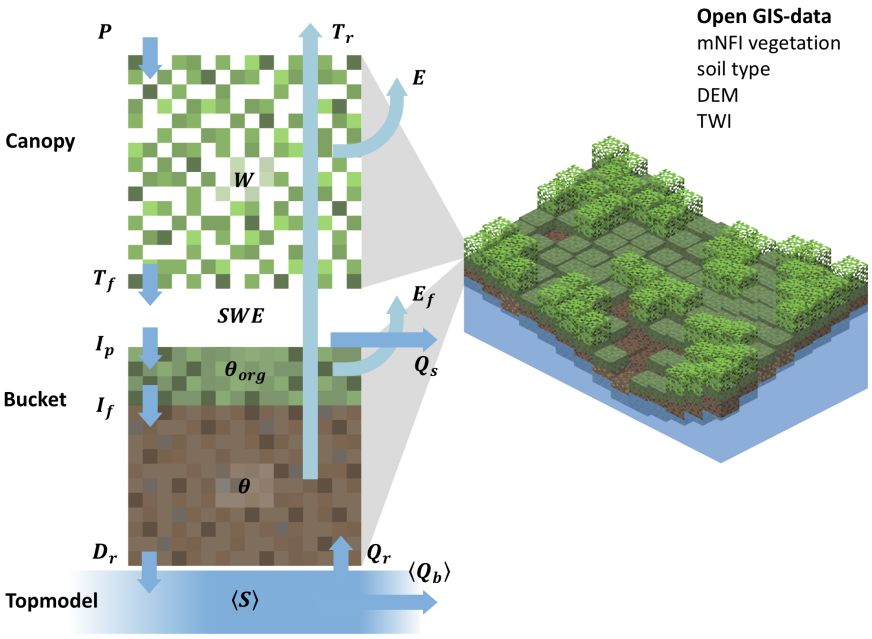

Figure 1. Structure of SpaFHy. At each grid cell, above ground and topsoil hydrology is solved by *Canopy* and *Bucket* sub-models whereas lumped *Topmodel* is used to model saturated zone. The arrows correspond to interfacial fluxes: P precipitation; T_f throughfall to virtual snowpack; I_p potential infiltration to organic layer; I_f infiltration to root zone; D_r drainage to saturated zone; E evaporation/sublimation of canopy storage; E_f evaporation from ground; T_r transpiration; Q_r returnflow; Q_s surface runoff; $\langle Q_b \rangle$ baseflow.

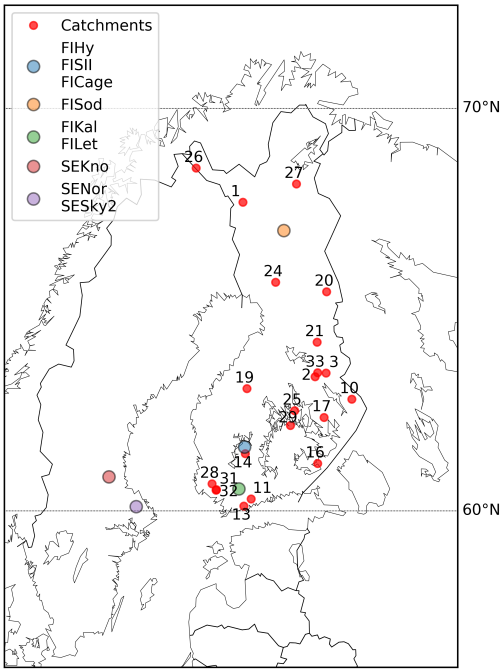

Figure 2. Location of the forest and peatland eddy-covariance sites and the 21 boreal headwater catchments used in the study.

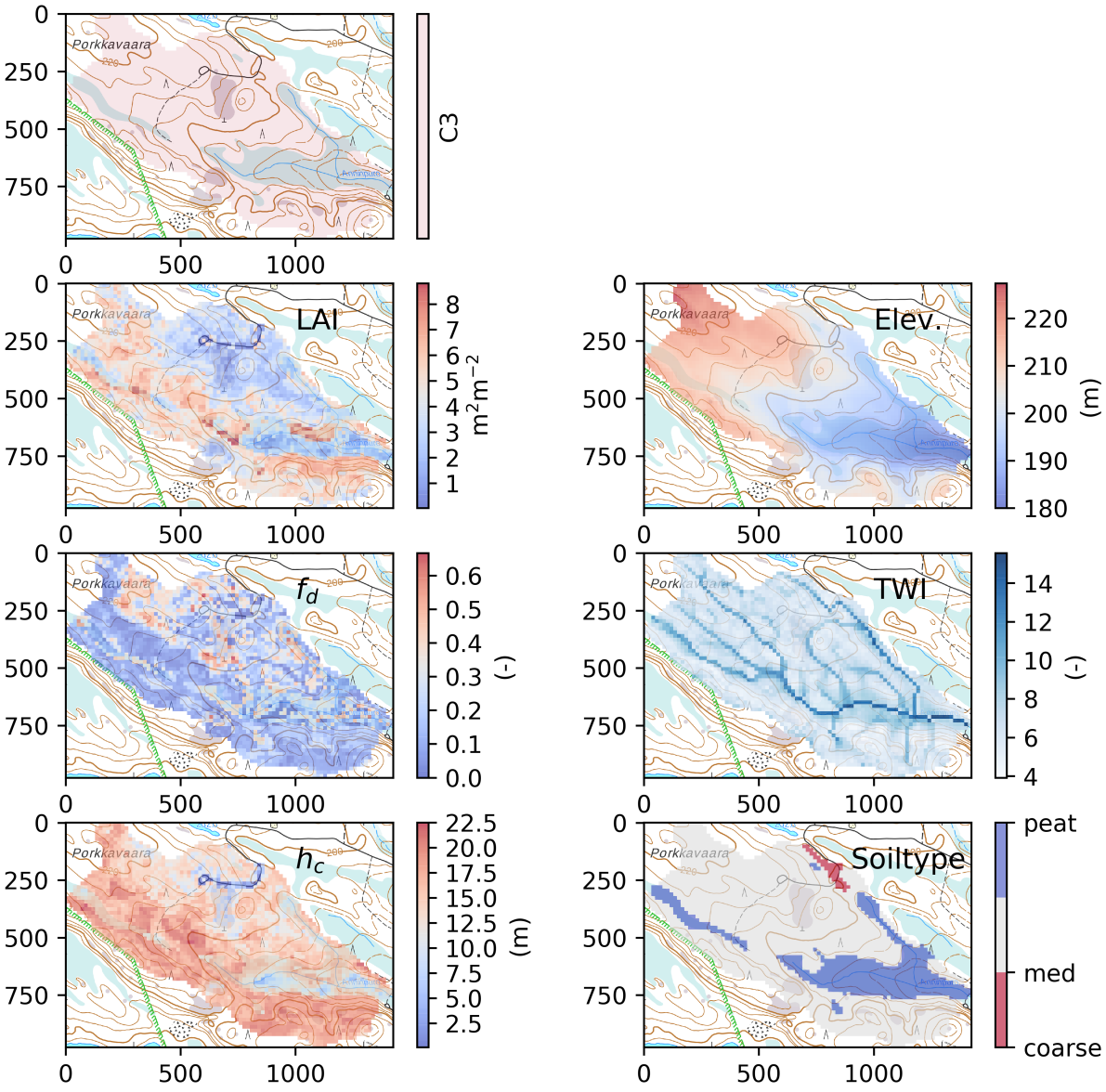

Figure 3. Spatial data at 16 m resolution used to set up the model for the catchment C3 Porkkavaara in Eastern Finland (see Table S2). LAI is total 1-sided leaf-area index; f_d deciduous fraction; h_c canopy height; Elev elevation; TWI topographic wetness index; soiltype refers to Table S2. Rasters overlay topographic basemap provided by National Survey of Finland and the scale of x and y axis is meters.

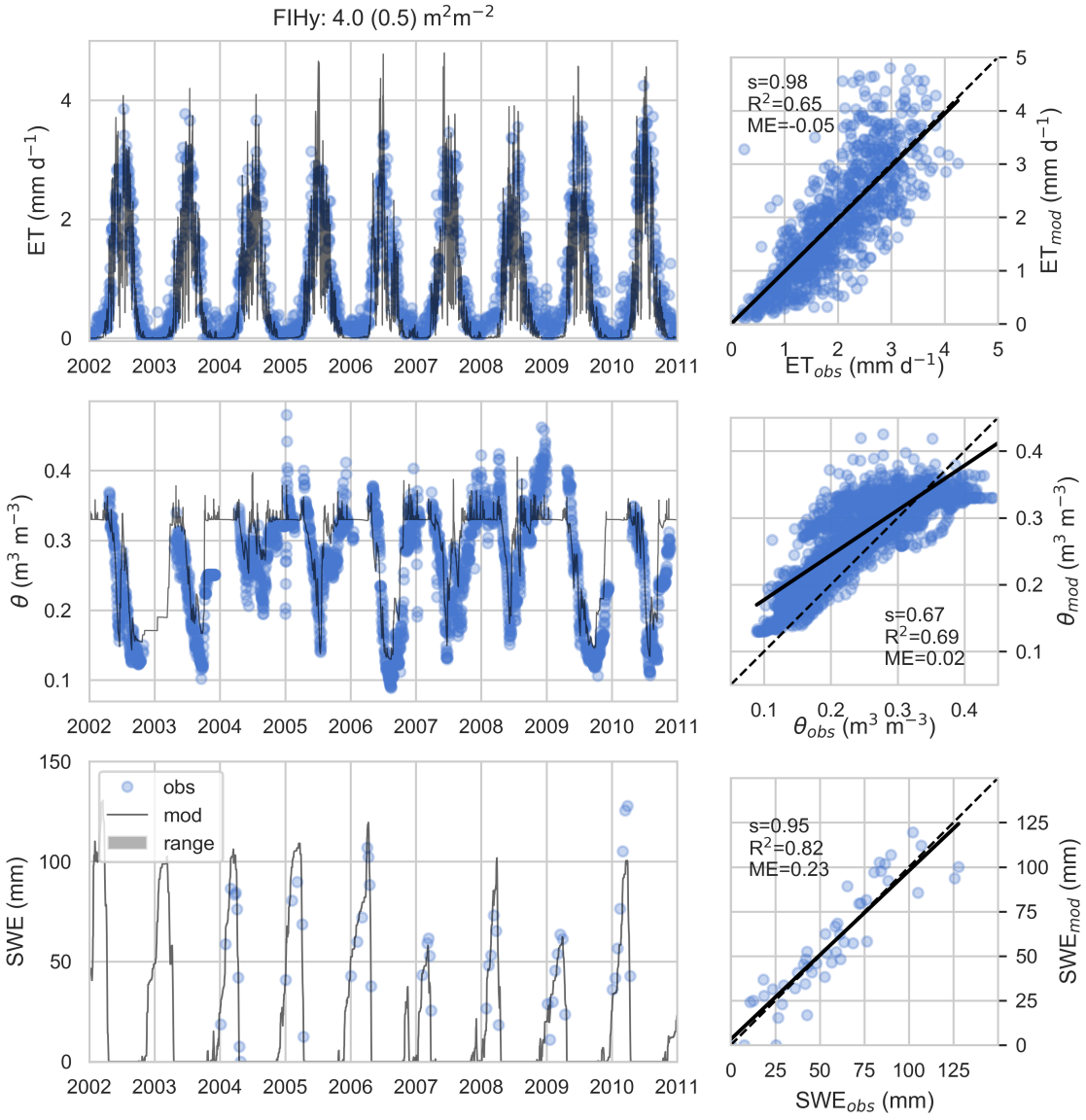

Figure 4. Modeled vs. measured dry-canopy ET at FIHy (top), root zone water content θ (middle) and snow water equivalent SWE (bottom). As soil freezing is not modelled, comparison of θ is restricted to conditions when measured soil temperature was $\geq 0°C$.

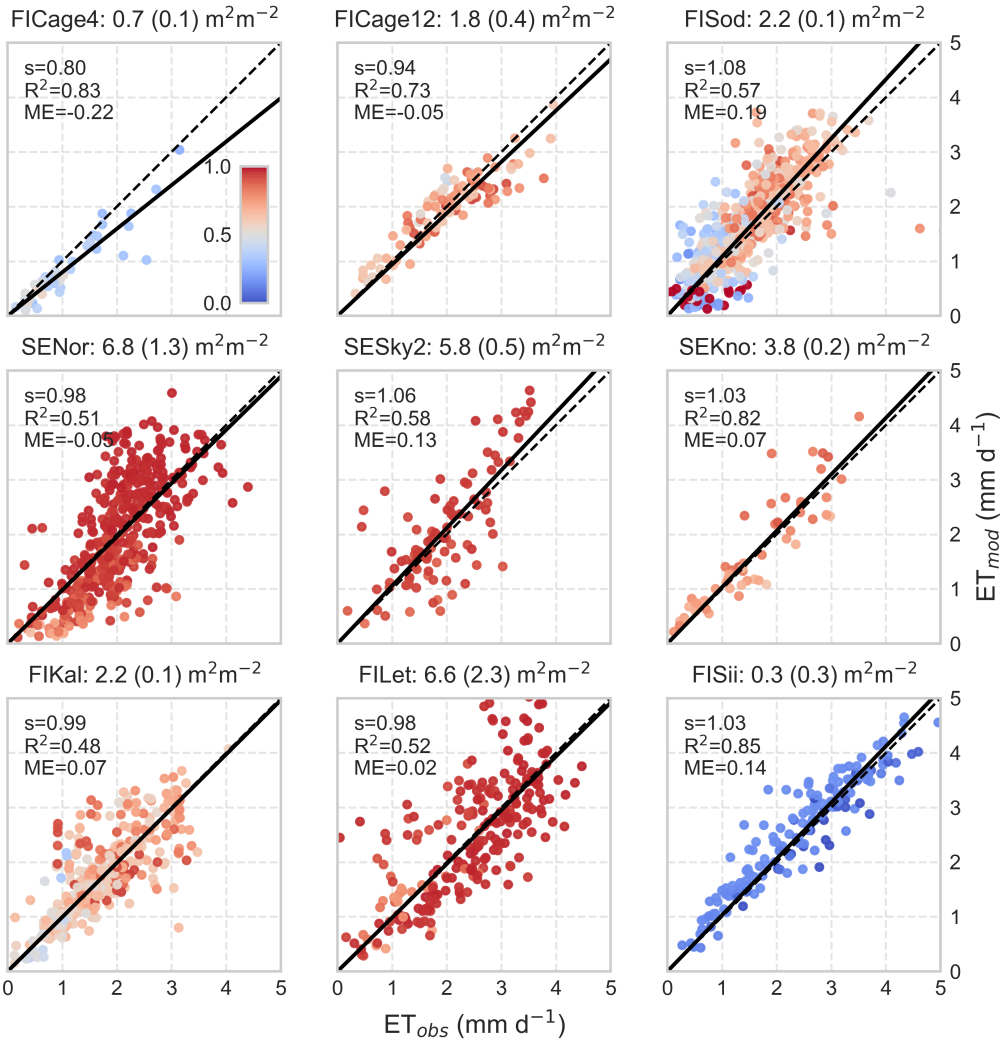

Figure 5. Scatter plots between modeled and observed daily stand-level ET during growing-season at the eddy-covariance flux sites in Finland and Sweden (Table 2). The title of each panel shows LAI (maximum deciduous LAI in parenthesis). The slope s and R^2 of linear regression forced through the origin and mean error ME are given and dashed line is the 1:1 line. Only dry canopy conditions, i.e. no rain during the day or previous day are included. At pristine fen peatland site FISii, E_f was assumed non-limited by organic layer moisture. Color coding is according to transpiration to ET -ratio $T_r/(T_r + E_f)$.

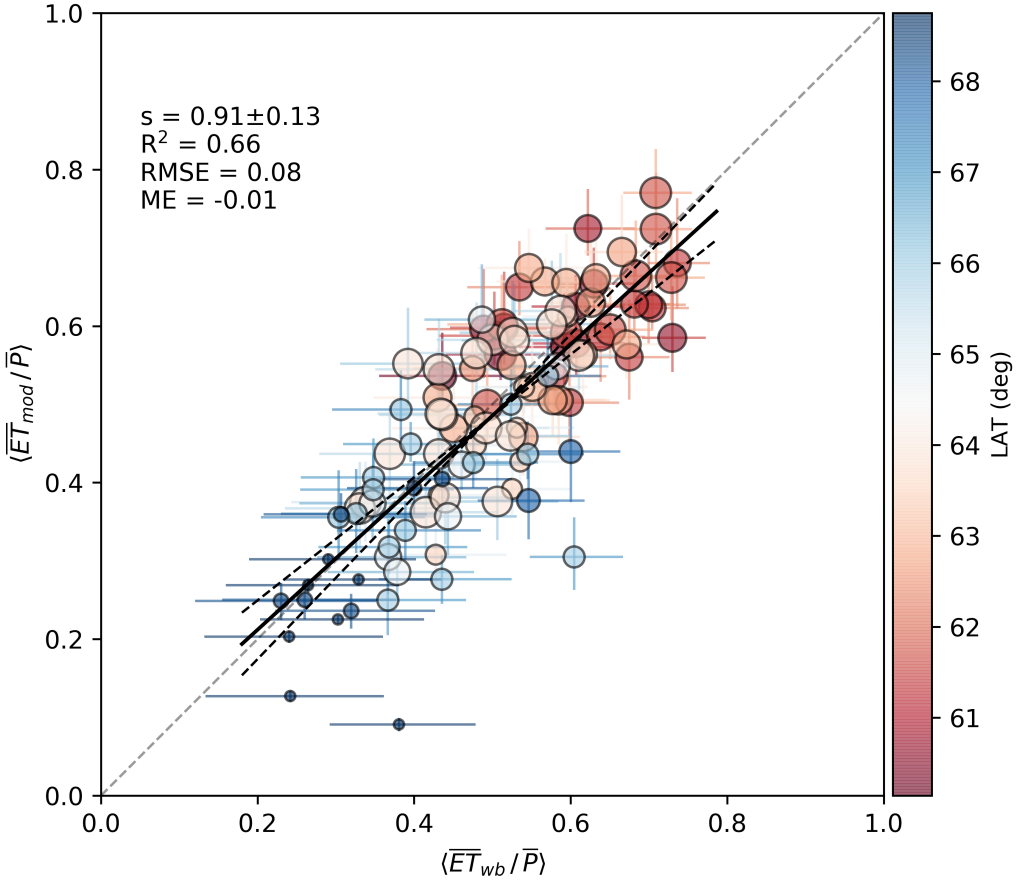

Figure 6. Modeled annual catchment evaporation fraction $\langle \overline{ET}_{mod}/\overline{P} \rangle$ compared to that inferred from catchment water balance $\langle \overline{ET}_{wb}/\overline{P} \rangle$. The vertical and horizontal errorbars show effect of parameter uncertainty and that of catchment area and P, respectively (see text). The colors refer to latitude and symbol size to catchment mean LAI (from 0.2 to 4.6 m^2m^{-2}). Using median year for each catchment (N=21), the respective statistics are: slope s 0.99±0.30, R^2 0.67, $RMSE$ 0.06, ME -0.003.

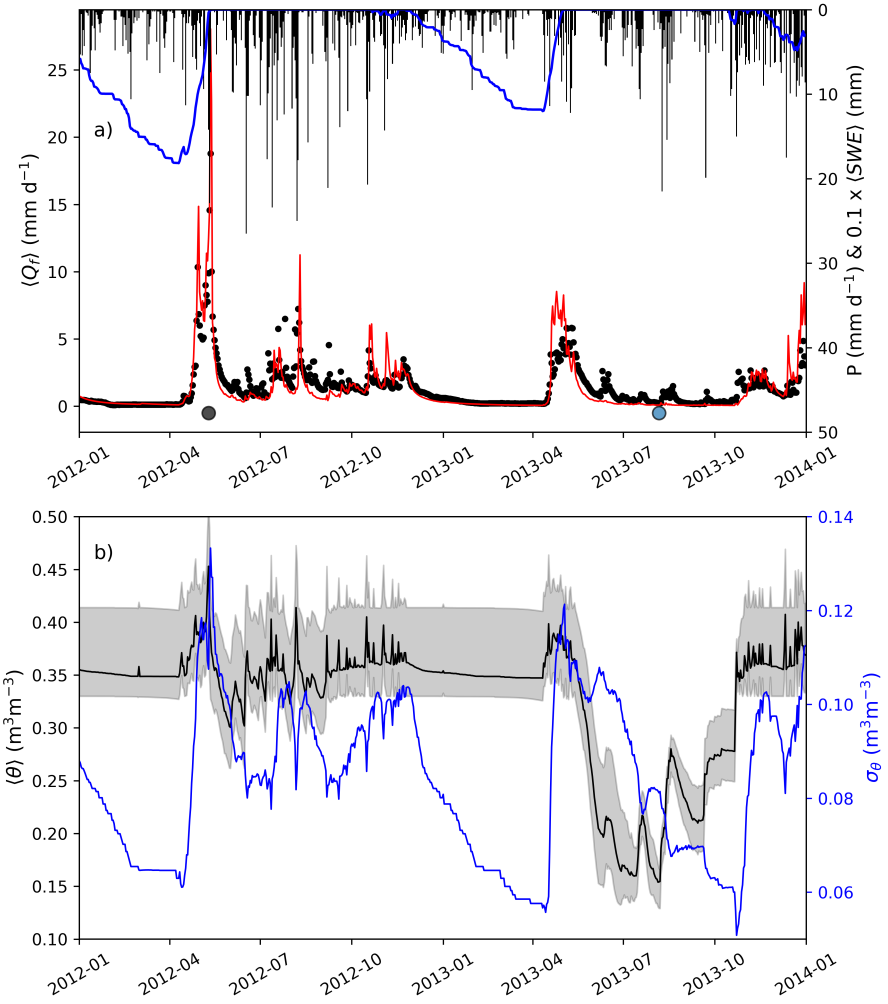

Figure 7. a) Measured (black) and modeled (red) specific discharge Q_f, daily precipitation P (black bars) and mean snow water equivalent SWE (blue); b) mean volumetric soil moisture $\langle\theta\rangle$ and its spatial standard deviation σ_θ (blue) over two hydrologically contrasting years at C3 Porkkavaara, Eastern Finland. In b) the the grey range shows the inter-quartile range. The points correspond to dates in Fig. 9. The Willmot's index of agreement (eq. 23) for specific discharge over 2012 - 2013 period is 0.77.

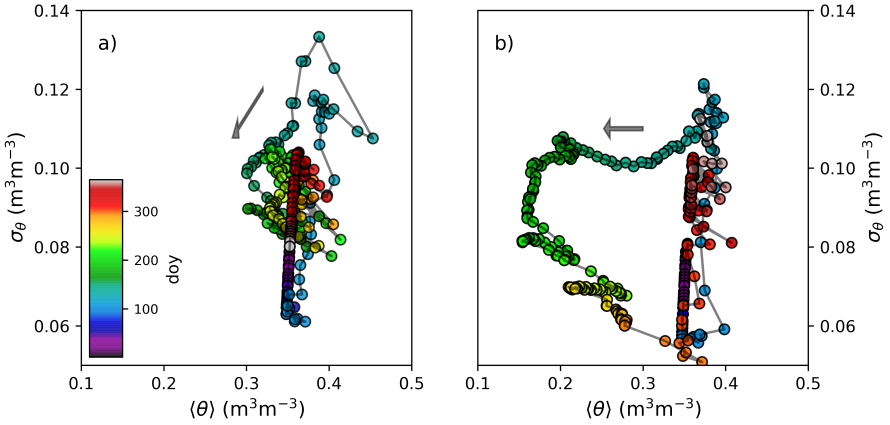

Figure 8. The relationship between catchment daily mean soil moisture $\langle\theta\rangle$ and its spatial standard deviation σ_θ over the course a wet (2012) and dry (2013) year at C3 Porkkavaara. The color scale shows day of year (doy).

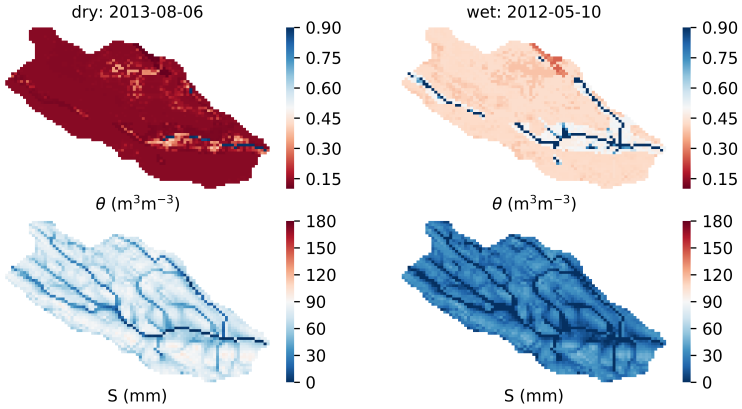

Figure 9. Snapshots of soil moisture patterns during wet and dry conditions (Fig. 7) at C3 Porkkavaara. Water content θ in the root zone (top) and local saturation deficit S of *Topmodel* (bottom).

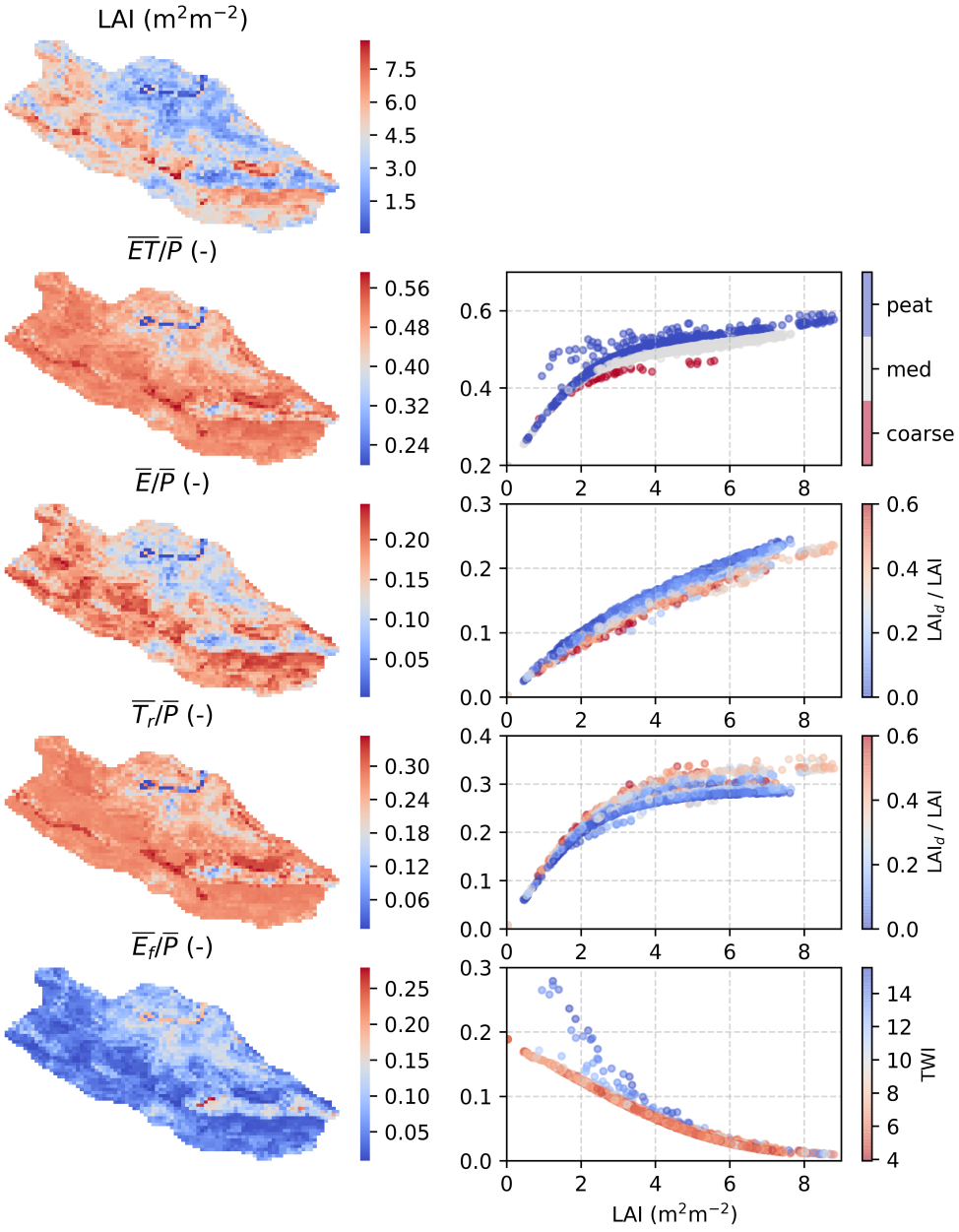

Figure 10. Spatial variability of evaporation fraction $\overline{ET/P}$ and its components at C3 catchment in Eastern Finland from a long-term (2006-2016) run (left). The relationship of component fluxes interception evaporation E, transpiration T_r and forest floor evaporation E_f on LAI (right) is modified with spatial variability of soil type, proportion of deciduous trees (LAI_d/LAI), and topographical wetness index (TWI).

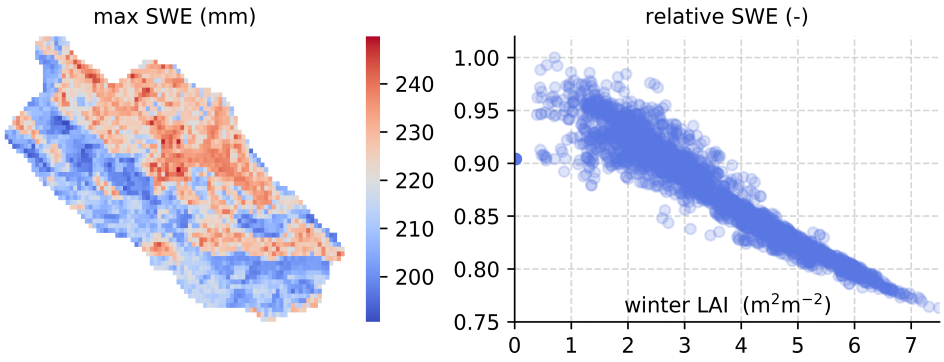

Figure 11. Spatial variability of maximum snow water equivalent (SWE) at C3 (left). The SWE relative to open area scales near-linearly with wintertime leaf-area index LAI (right).

Table 1. Generic parameter set used in stand and catchment scale simulations.

parameter	value	units	explanation	Note
Canopy				
A_{max}	10.0	μ mol m^{-2}s^{-1}	maximum leaf net assimilation rate	Suppl. material
$g_{1,c}$	2.1	kPa$^{0.5}$	stomatal parameter for conifers	shoot chamber in Launiainen et al. (2015)
$g_{1,d}$	3.5	kPa$^{0.5}$	stomatal parameter for deciduous	Lin et al. (2015), Suppl. material
b	50	W m^{-2}	half-saturation PAR of light response	Suppl. material
k_p	0.6	-	radiation attenuation coefficient	Suppl. material
r_w	0.20	-	critical relative extractable water	Lagergren and Lindroth (2002)
$r_{w,min}$	0.02	-	minimum relative conductance	assigned
G_f	0.01	m s^{-1}	surface conductance for evaporation from wet forest floor	calibrated
w_{max}	1.5	mm LAI^{-1}	canopy storage capacity for rain	calibrated
$w_{max,snow}$	4.5	mm LAI^{-1}	canopy storage capacity for snow	Pomeroy et al. (1998); Essery et al. (2003)
K_m	2.5	mm d^{-1}	melt coefficient in open area	Kuusisto (1984)
K_f	0.5	mm d^{-1}	freezing coefficient	Koivusalo and Kokkonen (2002)
Y_{max}	18.5	°C	phenology model parameter	Kolari et al. (2007b)
τ	13.0	d	time constant	Kolari et al. (2007b)
$T_{0,y}$	-4.0	°C	base temperature	Kolari et al. (2007b)
Bucket				
$z_{s,org}$	0.05	m	organic layer depth	assigned
$\theta_{s,org}$	0.90	-	porosity of org. layer	Laurén and Heiskanen (1997)
$\theta_{fc,org}$	0.30	-	field capacity of org. layer	Laurén and Heiskanen (1997)
z_s	0.4	m	root zone depth	Kalliokoski et al. (2010)
θ_s		m^{3}m^{-3}	porosity of root zone layer	soil type
θ_{fc}		m^{3}m^{-3}	field capacity of root zone layer	soil type
θ_{wp}		m^{3}m^{-3}	wilting point of root zone layer	soil type
K_{sat}		m s^{-1}	saturated hydraulic conductivity	soil type
β		-	decay parameter of hydraulic conductivity	soil type
Topmodel				
T_o	0.001	m s^{-1}	transmissivity at saturation	assigned
m	Catchment specific	m	effective soil depth	calibrated against discharge

Table 2. Eddy-covariance sites used in stand-scale validation

Site	Name	Lat Lon	Site type	LAI (m^2m^{-2})	Height (m)	Age (yr)	P (mm)	T_a (C)	Years	Soil	Reference
FIHy	Hyytiälä	61.85N, 24.30E	Scots pine mineral soil	4.0 (0.5)	15 (2)	45 (5)	709	2.9	2000-2005 2007-2010	medium texture*	Hari and Kulmala (2005) Launiainen et al. (2015)
FICage4	Hyytiälä 4yr	61.85N, 24.30E	Scots pine mineral soil	0.6 (0.1)	0.4 (0.2)	4 (1)	709	2.9	2000	medium texture	Rannik et al. (2002) Kolari et al. (2004)
FICage12	Hyytiälä 12yr	61.85N, 24.30E	Scots pine mineral soil	1.8 (0.4)	1.7	12 (1)	709	2.9	2002	medium texture	Kolari et al. (2004)
FISod	Sodankylä	67.36N, 26.64E	Scots pine mineral soil	2.2 (0.2)	13 (1)	150 (50)	527	-0.4	2001-2009	coarse texture	Aurela (2005), Thum et al. (2007)
FIKal	Kalevansuo	60.65N, 23.96E	Drained peatland	2.5 (0.5)	15 (1)	40 (3)	606	4.6	2005-2008	peat	Lohila et al. (2011)
FILet	Lettosuo	60.64N, 23.96E	Drained peatland	6.6 (2.3)	20 (2)	40 (3)	627	4.6	2010-2012	peat	Koskinen et al. (2014)
SENor	Norunda	60.09N, 17.48E	Mixed coniferous, mineal soil	6.5 (1.3)	27 (3)	100 (20)	527	5.5	1996, 1997, 2003	medium texture	Lundin et al. (1999) Lindroth et al. (2008)
SEKno	Knottåsen	61.0N, 16.22E	Norway spruce mineral soil	3.6 (0.2)	16.5 (1)	40 (3)	613	3.4	2006, 2009	medium texture	Berggren et al. (2004), Lindroth et al. (2008)
SESky2	Skyttorp 2	60.13N, 17.84E	Scots pine mineral soil	5.3 (0.5)	15.8 (1)	39 (2)	527	5.5	2005	medium texture	Gioli et al. (2004)
FISii	Siikaneva	61.85N, 24.30E	Boreal fen	0.3 (0.3)	0.3		709	2.9	2011, 2013, 2015	peat	Alekseychik et al. (2017)

LAI is ecosystem 1-sided leaf-area index (deciduous LAI in parenthesis); P is mean annual precipitation; T_a mean annual air temperature and soil type refers to Table 2 in the main document.

* for runs at FIHy, site-specific field capacity $\theta_{fc} = 0.3$ and wilting point $\theta_{wp} = 0.1$ corresponding to main root zone (Launiainen et al., 2015) were used.

Table 3. Parameters and their ranges used in the global sensitivity analysis (Morris method) at stand scale.

canopy parameters	range	unit	explanation
LAI	0.1 - 8.0	$m^3\ m^{-3}$	total leaf area index
f_d	0.0 - 1.0	-	deciduous fraction
g_1	1.0 - 7.0	-	stomatal parameter
A_{max}	6.0 - 14.0	μmol m^{-2} (leaf) s^{-1}	maximum leaf net assimilation rate
b	20.0 - 60.0	W m^{-2}	half-saturation PAR of light response
k_p	0.4 - 0.6	-	radiation attenuation coefficient
r_w	0.05 - 0.50	-	critical relative extractable water
G_f	1.0×10^{-3} - 1.0×10^{-1}	m s^{-1}	surface conductance for evaporation from wet forest floor
h_c	1.0 - 30.0	m	canopy height
w_{max}	0.5 - 3.0	mm LAI^{-1}	canopy storage capacity for rain
$w_{max,snow}$	1.0 - 10.0	mm LAI^{-1}	canopy storage capacity for snow
bucket parameters			
z_s	0.2 - 0.7	m	root zone depth
$z_{s,org}$	0.02 - 0.1	m	organic layer depth
$\theta_{fc,org}$	0.2 - 0.4	$m^3\ m^{-3}$	field capacity of org. layer
$\theta_{crit,org}$	0.1 - 0.4	$m^3\ m^{-3}$	critical vol. water content of org. layer

Table 4. Sensitivity of *Canopy* sub-model predictions to parameter variability. Mean (μ) and standard deviation (σ) of the distribution of elementary effects for evapotranspiration (ET), transpiration (T_r), evaporation from canopy interception (E), ground evaporation (E_f), and annual maximum snow water equivalent (SWE). Negative sign of μ indicate output variable decreases when parameter value increases. Units are in mm a^{-1} except for SWE (mm).

	ET		T_r		E		E_f		SWE	
Parameters	μ	σ	μ	σ	μ	σ	μ	σ	μ	σ
LAI	100	230	240	280	140	94	-130	77	-36	33
f_d	-9.5	13	-20	16	-32	14	11	8.3	23	21
g_1	97	82	97	82	0.0	0.0	-0.0	+0.0	0.0	0.0
A_{max}	56	38	56	38	0.0	0.0	-0.0	0.1	0.0	0.0
b	-42	23	-42	23	0.0	0.0	+0.0	+0.0	0.0	0.0
k_p	-3.3	13	20	19	0.2	0.1	-23	15	-0.2	0.1
r_w	-7.3	6.6	-7	6.6	0.0	0.0	0.0	0.0	0.0	0.0
G_f	17	52	-2.2	5.9	0.0	0.0	19	53	0.0	0.0
h_c	-8.2	29	-9.0	2.0	20	24	0.7	13	-4.4	4.9
w_{max}	-22	22	-19	23	69	43	-2.7	2.3	5.7	4.4
$w_{max,snow}$	-0.9	2.0	-1.9	2.3	11	14	1.0	0.8	-28	21
z_s	58	44	58	44	0.0	0.0	-0.1	0.3	0.0	0.0
$z_{s,org}$	19	24	-3.2	5.6	0.0	0.0	22	24	0.0	0.0
$\theta_{fc,org}$	7.8	8.5	-1.1	2.0	0.0	0.0	8.9	8.5	0.0	0.0